VARIATION IN THERMAL STRUCTURE AND GEOSTROPHIC CURRENT BETWEEN ALASKA AND HAWAII DETERMINED FROM SYNOPTIC SPACE SECTIONS

by

George Keith Gowans

United States
Naval Postgraduate School

THESIS

VARIATION IN THERMAL STRUCTURE
AND GEOSTROPHIC CURRENT BETWEEN ALASKA AND HAWAII
DETERMINED FROM SYNOPTIC SPACE SECTIONS

by

George Keith Gowans

October 1969

Variation in Thermal Structure and Geostrophic Current Between Alaska and Hawaii Determined from Synoptic Space Sections

by

George Keith Gowans
Lieutenant Commander, United States Navy
B.A., University of Mississippi, 1957

Submitted in partial fulfillment of the
requirements for the degree of

MASTER OF SCIENCE IN OCEANOGRAPHY

from the

NAVAL POSTGRADUATE SCHOOL
October 1969

ABSTRACT

Five synoptic space sections along 158°W longitude between Hawaii and the Aleutian Islands were developed from data collected by airborne expendable bathythermographs during experiment PARKA, a research project sponsored by the U. S. Navy in 1968. The sections are examined for spacial and temporal variation in thermal structure and geostrophic surface velocity.

Two recently developed analysis techniques are employed. Denner's T-S gradient method, wherein thermal and haline contributions to total geostrophic velocity are distinguishable, expedites calculations and results in velocity fields comparable to those developed by the dynamic method. Thermocline parameters are developed using Boston's objective definition of the thermocline, a statistical curve-fitting technique which develops the notion of a Gaussian thermocline.

Gross features of thermal structure remain fairly consistent during the heating season; however, thermal fronts are observed to vary in time and space. The distribution of isothermal lines with latitude suggests the possibility of a Taylor-column effect slightly north of Hawaii.

TABLE OF CONTENTS

LIST OF TABLES

LIST OF FIGURES

ACKNOWLEDGEMENTS

The author acknowledges with gratitude the guidance and patience offered unstintingly by Assistant Professor N. E. J. Boston during the preparation of this thesis. In his capacity as faculty advisor, it fell to him the onerous task of unscrambling the convoluted syntax and portentious pronouncements of which novice graduate students are so enamored.

The generous donation by Dr. W. W. Denner of his valuable time and advice was invaluable to the orderly completion of the task at hand.

Special thanks are extended to the officers and staff of the Fleet Numerical Weather Central, Monterey, California for their kind cooperation in providing data and assistance whenever requested; the interest expressed in the project and the helpful suggestions offered by Dr. T. Laevastu were particularly appreciated.

A final but most sincere note of appreciation is extended to Mr. B. R. Mendenhall of Meteorology International Inc., Monterey, California for his active interest in and support of this project.

I. INTRODUCTION

The genesis of this investigation was experiment PARKA - a research project sponsored by the Oceanographer of the Navy to investigate the acoustic environment in the mid North Pacific Ocean. The objectives of PARKA were many and varied and are largely inappropriate for discussion here. More to the point is the large body of environmental data accumulated during the execution of the project.

The principal phases of PARKA were conducted in August and September 1968. During this period more than 2,000 observations were recorded along a line approximately corresponding to 158°W longitude between 22-55°N latitude. More than ten surface ships (including the floating instrument platform FLIP) together with Navy patrol aircraft participated in the experiment. Because of the acoustic nature of the mission, the program of environmental data collection was designed primarily to determine thermal structure. To this end, a variety of instruments were used: mechanical bathythermographs (BT), shipborne (XBT) and airborne (AXBT) expendable bathythermographs, airborne radiation thermometers (ART), and *in situ* salinity, temperature, depth recording devices (STD). Salinity structure along the track was defined from climatological atlases augmented by a limited number of real-time profiles recorded by STD.

Considered in total, the PARKA data define the thermal structure in the upper 300m of a hydrographic section extending some 2,000 miles. The section is unique in two respects. First is the sheer number of observations wherein thermal parameters were determined independently

and often simultaneously by several different instruments. Secondly, the sections developed from AXBT records are as nearly synoptic as possible - roughly 70 profiles along the entire track completed in eight hours.

The most intriguing aspect of PARKA for the author was the extensive use of the AXBT. The AXBT flights not only initiated the instrument in a major scientific undertaking but also produced the only known space sections of thermal structure on so large a scale. The entire track between Hawaii and the Aleutian Islands was traversed five times - four flights during the actual execution of PARKA and a follow-on mission two months later. The fifth transit was completed 23 November 1968; thus the time frame of the flights includes the end of a heating season and the first one-third of a cooling season. Five sections developed from data collected during these flights form the basis for this study.

Each section was examined to determine latitudinal variation of selected isotherms and of the depths to the top, center, and bottom of the thermocline. One section was selected for geostrophic computations by both the dynamic method (Proudman, 1953) and the T-S gradient method (Denner, 1969) to compare resulting surface velocity fields. A correlation between total surface velocity and its thermal contribution, as calculated by the T-S gradient method, was attempted in order to develop geostrophic velocity fields in the remaining sections based solely on thermal structure.

With the spacial variation of the indicated parameters established, the five sections were considered together in order to develop the objectives of this thesis. Briefly stated, these objectives are: to examine the spacial and temporal variation of the top, center and

bottom of the thermocline; to examine the spacial and temporal variation of selected isotherms, correlating the results to thermocline variations; to test the T-S gradient method as a device for rapid and realistic dynamic calculations; and to examine the AXBT as a scientific instrument.

In developing these objectives, two fairly recent inovations are employed. The first, already mentioned, is the T-S gradient method wherein the thermal and haline contributions to geostrophic velocity are distinguishable. The second is the notion of a "Gaussian thermocline" developed by Boston (1966). In order to bring the results developed from these two techniques into sharper focus - as well as to evaluate the reliability of the AXBT - this thesis considers exclusively the temperature and depth data provided by airborne thermograms. The assumption is that if reasonable results can be developed solely from temperature data, the subjective application of atmospheric effects at the air/sea interface will only enhance the value of the results.

II. DISCUSSION OF THE DATA

Temperature data were collected during five flights by Navy P-3 patrol aircraft. Altitude and airspeed varied somewhat among missions, depending on flying conditions, but remained well within limits for efficient operation of the AXBT. Altitudes generally ranged between 2,000-5,000 feet and airspeeds between 200-250 knots.

A. AREA COVERAGE

Each of the five flights originated in the Aleutian Islands and terminated in Hawaii. Flight plans were the same for each mission. The track extended 1,985 nautical miles along $157^{o}50'W$ longitude between $55^{o}05'N$ and $22^{o}00'N$ latitude. Figure 1 is a representation of the cross section along the track. Take-off time was scheduled to ensure arrival of the aircraft on the track one hour either side of 0800 local time. Optimum spacing between observations was set at 25nmi which corresponds to an instrument launching about every six minutes.

All flights conformed to the track within navigational error and the instrument launching schedule was followed as closely as practicable. Spacing between temperature profiles along the track was ultimately a function of the quality of the thermograms; only those traces extending to 300m or greater were considered. The lack of uniformly spaced observations does not inhibit development of the objectives outlined earlier.

Table I is a summary of pertinent time and space factors describing each section; the indicated number of observations are those that met the 300m criterion and were free from obvious errors.

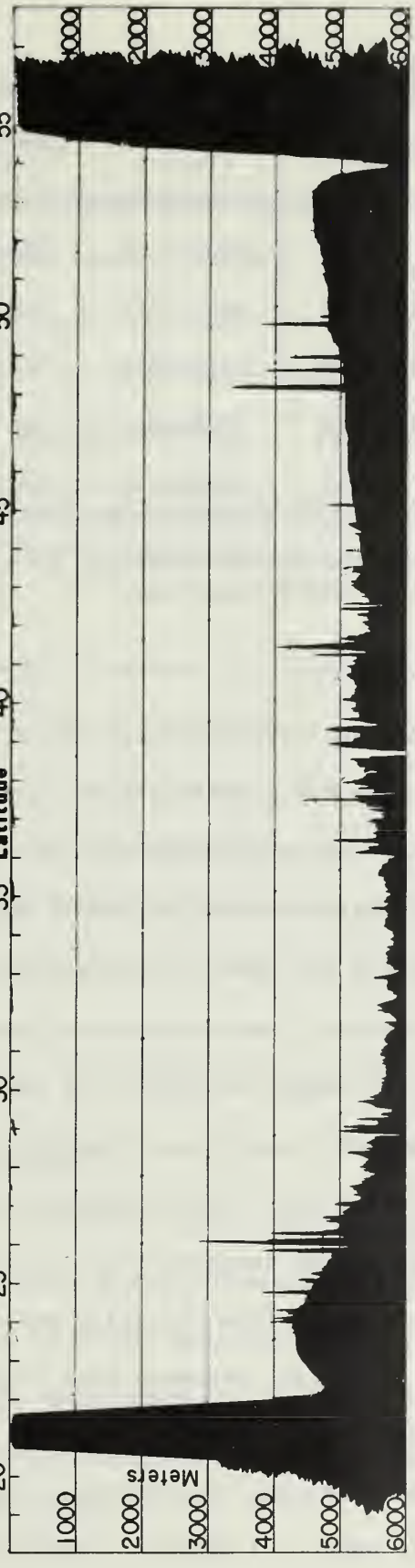

Figure 1. Cross section of PARKA track.

SECT	DATE	TIMES (local)	COVERAGE (^{o}N lat)	OBS
1	19 Aug 68	0809-1630	54.1-22.3	70
2	22 Aug 68	0807-1621	54.7-22.6	72
3	2 Sept 68	0810-1636	54.6-22.1	67
4	4 Sept 68	0810-1649	54.7-22.2	69
5	23 Nov 68	0840-1746	53.9-22.0	55

TABLE I. Time and space dimensions of synoptic sections along 158^{o}W longitude.

B. INSTRUMENTATION

The instrument package carried aboard the aircraft included AN/SSQ-36 Bathythermograph Transmitter Sets (herein referred to as AXBT) and an Anadex Converter-Rustrack Recorder Assembly (NADC Converter) used in conjunction with an AN/ARR-52 Radio Receiving Set.

As the name implies, the AXBT is an expendable aircraft launched device designed to provide a sea temperature profile from the surface to a depth of 1,050 ft. Major components of the instrument are a temperature probe, an audio oscillator controlled by the probe, a timing circuit, batteries and a VHF transmitter. The total assembly is housed in a standard size sonobuoy case and weighs 18 pounds.

The AXBT may be launched from virtually any altitude; however, something less than 10,000 ft. produces best results. At an altitude of 3,000 ft., for example, a complete thermogram is recorded aboard the aircraft about 5.5 minutes after the instrument is launched; at 1,000 ft. the interval would be about 4.7 minutes. The instrument is stabilized

by a rotochute during decent. On impact, the bottom plate is released and the sea-water batteries become active. Approximately 75 seconds later, the timing circuit releases the temperature probe which sinks at a uniform rate of five feet per second. An audio signal whose frequency is proportional to temperature modulates the VHF carrier frequency during descent of the probe. The audio frequency varies from 1,300 to 2,700Hz corresponding to a temperature range of 25 to 95^{o}F. Primary voltage is removed from the transmitter about six minutes after entry into the water; a water-soluable plug dissolves soon thereafter allowing the instrument to sink.

The Anadex Converter receives the demodulated signal directly from the ARR-52 radio receiver and converts it to a voltage proportional to the frequency of the incoming signal. The converter output signal is supplied to the Rustrack Recorder where the signal amplitude developed by the converter is visually displayed on a recording chart. The chart drive is set at three inches per minute to allow in-flight interpretation if required.

The effectiveness of the AXBT is discussed in section V.

C. PROCESSING AND ANALYSIS

At the completion of each flight, the thermograms were delivered to a representative of Fleet Weather Center, Hawaii. All traces are forwarded eventually to the Fleet Numerical Weather Central (FNWC) in Monterey, California, where they are digitized and stored on tape. The ultimate repository for the traces is the Naval Oceanographic Office, Washington, D. C.

This processing has been completed for the thermograms defining sections 1-4 (see Tab. I). Traces from section five were interpreted at the Hawaii Institute of Geophysics and results transmitted electronically to FNWC. Digitized versions of these traces were not available at this writing.

All observations are coded as a series of linear segments. In the case of the digitized data, the CDC 6500 computor at FNWC was programed to report temperature/depth pairs so that temperature deviated from linearity by no more than $0.075^{o}C$ between reported levels. The data transmitted electronically from Hawaii reported depths and associated temperatures of observed points of inflection in the traces.

All data were punched on cards for processing by the Naval Postgraduate School IBM 360 computor. A linear interpolation scheme was devised to permit temperature determinations at more convenient depths.

Thermocline calculations were made using subroutines developed by Grosfils (1968) following Boston (1966). Algorithms for computing geostrophic velocity were written by Mr. R. L. Middleburg of the Department of Oceanography, Naval Postgraduate School, and are presented by Denner (1969). The contours of isothermal lines were plotted by Subroutine METMAP from the IBM library at the Naval Postgraduate School.

III. GEOSTROPHIC MOTION ALONG 158°W LONGITUDE

Geostrophic calculations by the classical dynamic method are described in any of several textbooks on physical oceanography, for example Proudman (1953) or Neumann and Pierson (1966). The limitations and computational errors inherent in the dynamic method are summarized by Denner (1969). As an alternative to the dynamic method, Denner has developed a simplified scheme in which geostrophic velocity is expressed as three terms involving the observed variables, salinity and temperature. A useful feature of the method is that the thermal (V_t) and haline (V_h) contributions to total geostrophic velocity (V_g) are calculated separately. The import of this valuable feature is the possibility for rapid geostrophic calculations based solely on thermal structure - provided a correlation between V_g and V_t can be established. Such a correlation was determined by Moynihan (1968) in two water masses in the Grand Banks area. He pointed out the tangible benefits that would accrue to the International Ice Patrol if geostrophic velocity fields could be determined from a network of stations occupied by bathythermographs alone, making use of the high ship speeds permitted by use of the XBT. Granting this, even greater savings in time and effort would result from the use of airborne rather than surface instrument platforms.

Accordingly, this section briefly describes the development of the T-S gradient method and applies the technique to the AXBT data.

A. THE T-S GRADIENT METHOD

Assuming that sea water can be considered a binary fluid system, Denner followed Reid (1959) in observing that the Helland-Hansen

equation for geostrophic flow between two stations can be expressed:

$$(V_1-V_2) = \frac{1}{f}\int_{P_1}^{P_2}\left[\left(\frac{\partial a}{\partial T}\right)_{S,P}\frac{dT}{dn} + \left(\frac{\partial a}{\partial S}\right)_{T,P}\frac{dS}{dn}\right]_P dP \qquad (1)$$

where:

n = the horizontal distance between stations;

f = the Coriolis parameter;

a = specific volume as a function of salinity, temperature, and pressure;

(V_1-V_2) = magnitude of the relative current normal to n.

The subscript P indicates the bracketed quantity is evaluated at constant pressure.

Equation 1 expresses the geostrophic velocity in terms of three essential elements:

Horizontal gradients of temperature and salinity;

A quantity specifying the dependence of specific volume on temperature at a given salinity and pressure; and

A quantity specifying the dependence of specific volume on salinity at a given temperature and pressure.

Note that the specific volume terms in (1) become the coefficients of thermal compressibility and saline contraction if each is divided by specific volume; compressibility of sea water enters the equation indirectly through the dependence of these quantities on pressure.

Using (1) as a departure point, Denner examined several possibilities for developing tractable expressions for the specific volume terms. The approach selected was to compute specific volume at varying values of temperature, salinity and pressure using the Ekman equation of state for sea water and fitting the results with polynomials in the least

squares sense. The Ekman equation was selected because of its wide usage rather than any intrinsic superiority over other equations of state.

Values of specific volume were computed for all combinations of variables at prescribed intervals between 0-30°C temperature, 30-40°/oo salinity, and 0-200bar pressure. The resulting polynomials were of the form:

$$a(T)_{S,P} = a_o(S,P) + A(S,P)T + B(S,P)T^2 \tag{2}$$

$$a(S)_{T,P} = a_o(T,P) - C(T,P)S \tag{3}$$

where a_o is the specific volume at atmospheric pressure.

Differentiation of (2) and (3) with respect to temperature and salinity respectively yields expressions appropriate for substitution into (1). Effecting this substitution produces the following simplified expression for computing geostrophic currents, defined by Denner as the T-S gradient method:

$$(V_1 - V_2) = \frac{1}{f} \int_{P_1}^{P_2} \left[A(S,P) \frac{dT}{dn} + 2B(S,P)T \frac{dT}{dn} - C(T,P) \frac{dS}{dn} \right]_P dP \tag{4}$$

He pointed out that the interaction between the thermal and haline contributions to total flow takes place through the coefficients A(S,P), B(S,P), and C(T,P); therefore, the first two terms of (4) can be considered the thermal contribution and the last term the haline contribution to total flow. Interpolated values of the three coefficients as functions of their independent variables are displayed in graphic and tabular form in Denner's paper.

1. Computational Form

To extend application of the T-S gradient method, Denner demonstrated that weighted mean values of the three coefficients in (4) could be determined for large oceanic areas to facilitate calculation of geostrophic surface currents relative to a selected isobaric level. Equation 4 could then be rewritten in terms of finite differences for computation:

$$(V_1-V_2)_i = \frac{1}{f\Delta n}\left[\bar{K}_1 \sum_i \Delta T_i \Delta P_i + \bar{K}_2 \sum_i \bar{T}_i \Delta T_i \Delta P_i - \bar{K}_3 \sum_i \Delta S_i \Delta P_i\right] \qquad (5)$$

where:

$\bar{K}_1$, $\bar{K}_2$, $\bar{K}_3$ = weighted mean values of A(S,P), 2B(S,P), and C(T,P) respectively between the surface and the selected reference level (cgs units);

ΔT_i = average horizontal temperature difference in the i-th pressure interval (^oC);

$\bar{T}_i$ = average temperature in the i-th pressure interval (^oC);

ΔS_i = average horizontal salinity difference in the i-th pressure interval (o/oo);

ΔP_i = the i-th pressure interval (dynes/cm^2);

Δn = horizontal separation of the stations (cm).

Denner assigned fixed values to $\bar{K}_1$, $\bar{K}_2$, and $\bar{K}_3$ relative to the 1,000db surface in the Pacific Ocean after observing that average values of A(S,P), B(S,P) and C(T,P) calculated for summer and winter conditions did not vary greatly over the entire area or between seasons. The assigned values are:

$$\bar{K}_1 = 81.0 \times 10^{-6} \text{ (cgs units)}$$

$$\bar{K}_2 = 86.5 \times 10^{-7} \text{ (cgs units)}$$

$$\bar{K}_3 = -74.0 \times 10^{-5} \text{ (cgs units)}$$

Calculations using these fixed values introduced errors of not more than five percent in surface velocities computed from actual observations.

2. Application to AXBT Data

A preliminary step to the task implied in the heading of this section was to validate the correspondence between surface velocities determined by the dynamic method and by the T-S gradient method. AXBT section 2 was selected arbitrarily for the comparison. Salinity profiles corresponding to those of temperature were supplied by FNWC from historical data in their tape files. Absolute values of salinity were not important in that the same values were used in both methods; more germane was the characteristic variety of structural features provided by the profiles. Surface velocities were calculated by both methods for 72 station pairs; the pairs were formed by coupling adjacent stations in succession along the track. The relative error between results for each station pair was calculated by dividing the difference between the two velocities by the magnitude of the "dynamic" velocity and expressing the results as a percentage. Figure 2 illustrates the correlation between results.

The agreement was excellent. Over half of the 73 comparisons differed by less than two percent. Relative error exceeded five percent only at those points where calculated velocities were on the order of one centimeter per second. The introduction of large relative errors in regions of weak currents does not detract from the practicality of the T-S gradient method. Quite often it is sufficient merely to know that geostrophic currents are less than a few centimeters per second; this fact can be determined even if the relative error is large.

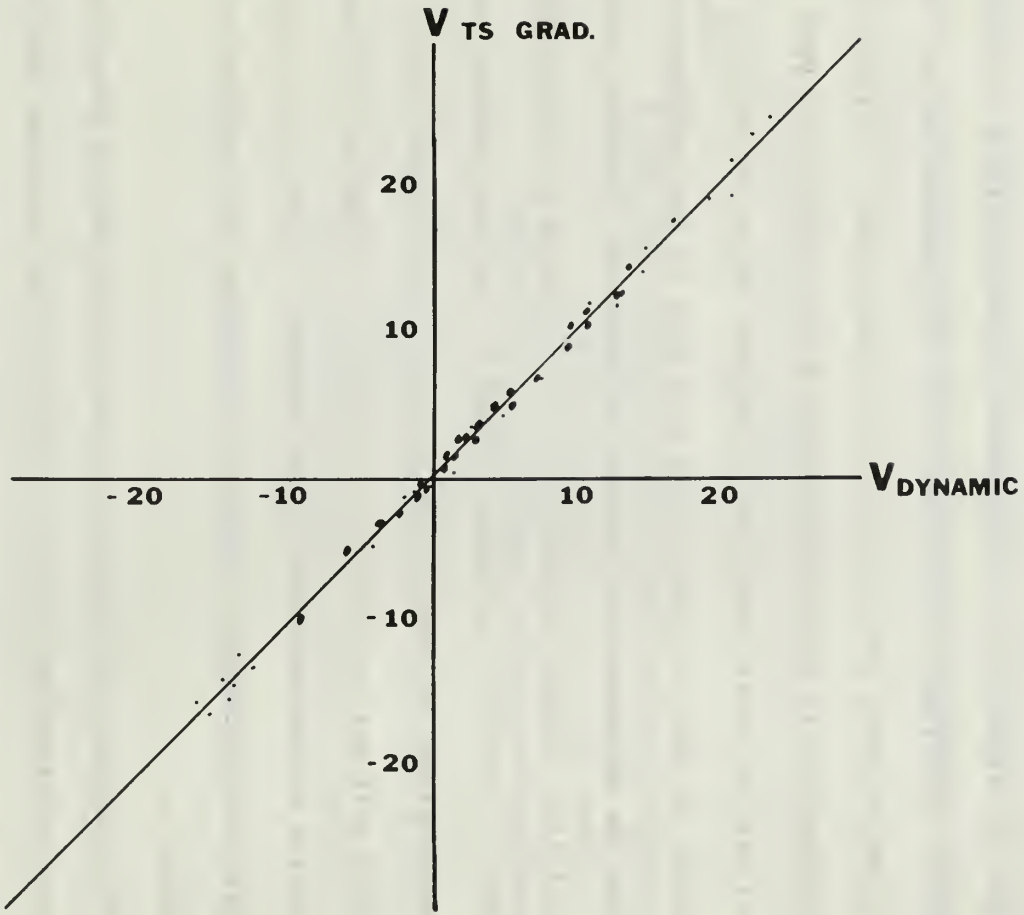

Figure 2. Correlation between dynamic and T-S gradient methods for computing geostrophic flow.

The question to be addressed next is whether or not a definitive relation exists between the geostrophic surface velocity and its thermal contribution. Throughout the remainder of this paper, references to geostrophic velocities or currents imply values calculated by the T-S gradient method.

a. Correlation Between V_g and V_t

Again, section 2 was selected to demonstrate correlation. V_g was calculated using (5); V_t was calculated using (5) less the third term on the right side. The reference level was set at 300m and the fixed values of the $\bar{K}$-constants determined by Denner were used. Initially, station pairs were formed in the same manner as described earlier, i.e. successive coupling of adjacent stations. The calculated velocities were fitted with a first-degree polynomial in the least square sense by digital computor using the IBM library subroutine LSQPOL. The resulting linear expression,

$$V_g = -0.880 + 1.040V_t$$

has a standard deviation of 3.44cm/sec. The average spacing between stations was on the order of 50km.

Reed and Laird (1966) point out that there is an optimum spacing between stations that should be considered when making geostrophic calculations. If calculations are made by the dynamic method, the spacing is determined by the maximum error acceptable in the results and the measurement error in determining the geopotential anomaly difference of the two stations. If the allowable error in the results is set at 20%, for example, the anomaly difference should be at least five times the measurement error. Thus, if measurement error is $\pm$ 1.1 dynamic centimeters, as they assumed, stations should be chosen such

that the anomaly difference is at least 5.5 dynamic centimeters. Table II presents the minimum station spacing recommended by Reed and Laird along two sections of the North Pacific, one of which (160°W) closely corresponds to the track considered here.

CURRENT	OPTIMUM STATION SPACING (km)	
	along approx. 160°W	along approx. 175°W
Alaska Stream	16	8
Subarctic	183	110
West Wind Drift	61	39
Gyre	> 137	> 137
Kuroshio Extension	55	34

TABLE II. Computed minimum distance between stations for near-surface geostrophic flow determinations. (After Reed and Laird, 1966.)

The relevance of the values in Table II to calculations other than by the dynamic method is not clear; unfortunately, time constraints prevented a more rigorous investigation of this point. In view of the objective of this section - to develop a rapid, simple method for determining geostrophic velocity fields - a compromise was struck. The computor was programed to select stations such that spacing was always greater than 100km. For section 2 the result was 25 station pairs with an average spacing on the order of 140km. The calculated velocities were again fitted to a first-degree polynomial. The resulting expression, equation (6), has a standard deviation of 2.473cm/sec.

$$V_g = -0.788 + 0.997V_t \qquad (6)$$

The improved value of standard deviation supports the notion of optimum spacing; additionally, the goodness of fit would seem to suggest that the horizontal distribution of temperature provides the major contribution to geostrophic velocity along 158°W longitude.

Geostrophic velocities were calculated for the five sections using (6); the results are presented in Figs. 3-7. Reed and Laird (1966) made similar calculations (using the dynamic method) from data collected between 1961-64 along approximately the same track. Figure 8 presents their results compared to actual current measurements.

B. LATITUDINAL VARIATION OF GEOSTROPHIC FLOW

A general pattern of eastward flow is evident in Figs. 3-7; relatively strong flow recurs at approximately 24, 27, and 34-36°N latitude. In Fig. 8, Reed and Laird indicate comparable movement at 24, 30 and 39°N latitude. Considering the difference in data and analysis technique, the agreement is remarkably good, both in location and magnitude. Two additional features which recur consistently in Figs. 3-7 are indications of weak westerly flow in the far north and stronger westerly flow in the far south. The former is quite likely a remnant of the Alaska Gyre, inducing a westerly velocity component at the convergence of the Alaska Stream and the Subarctic current (Tabata, 1965, Fig. 1). The mechanism producing the latter, however, is not clear. This point will be addressed further in the section discussing isotherm patterns. Aside from these features, the five velocity fields seem to differ most with respect to season.

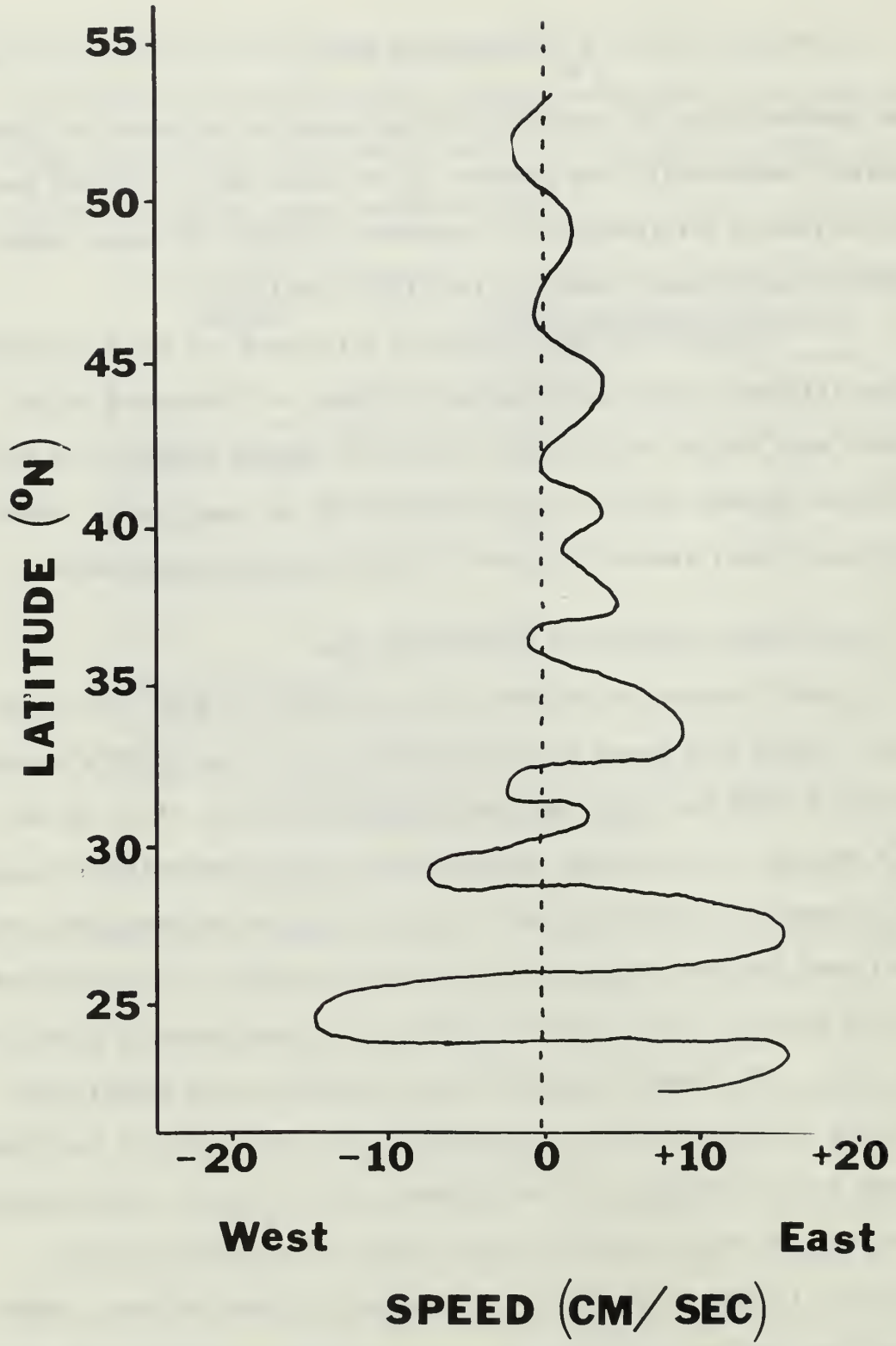

Figure 3. Latitudinal variation of geostrophic flow - 19 AUG 1968.

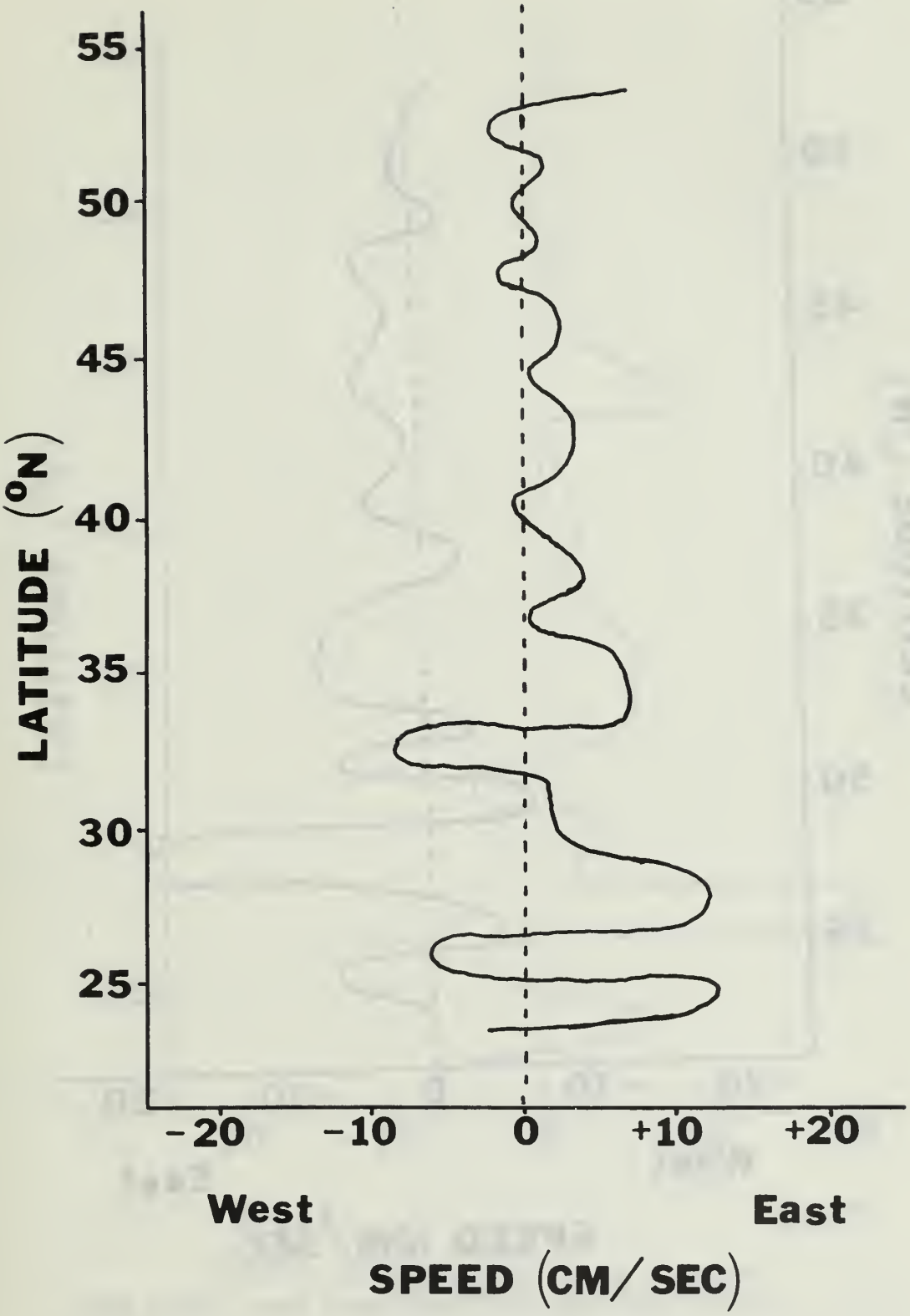

Figure 4. Latitudinal variation of geostrophic flow - 22 AUG 1968.

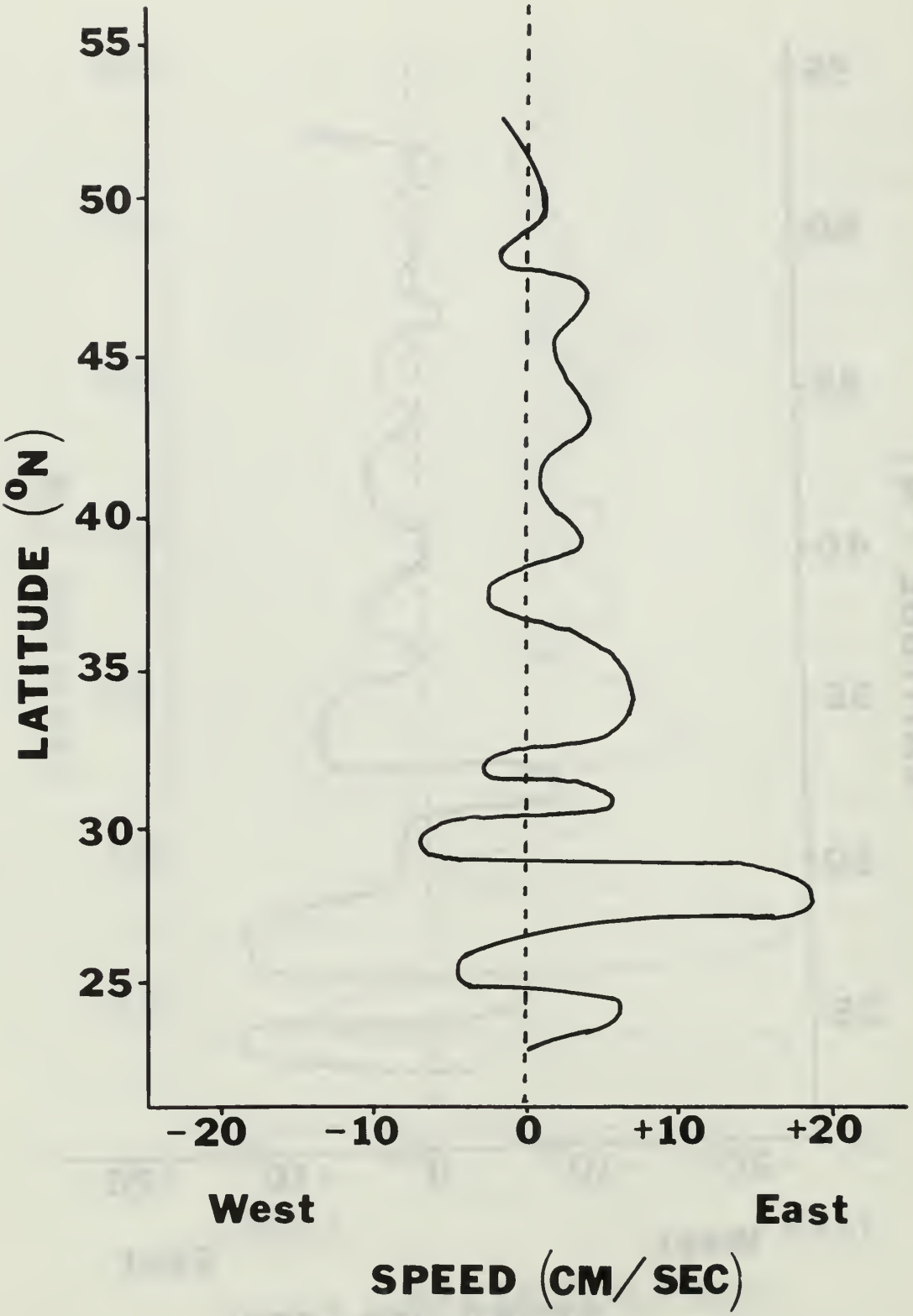

Figure 5. Latitudinal variation of geostrophic flow - 2 SEPT 1968.

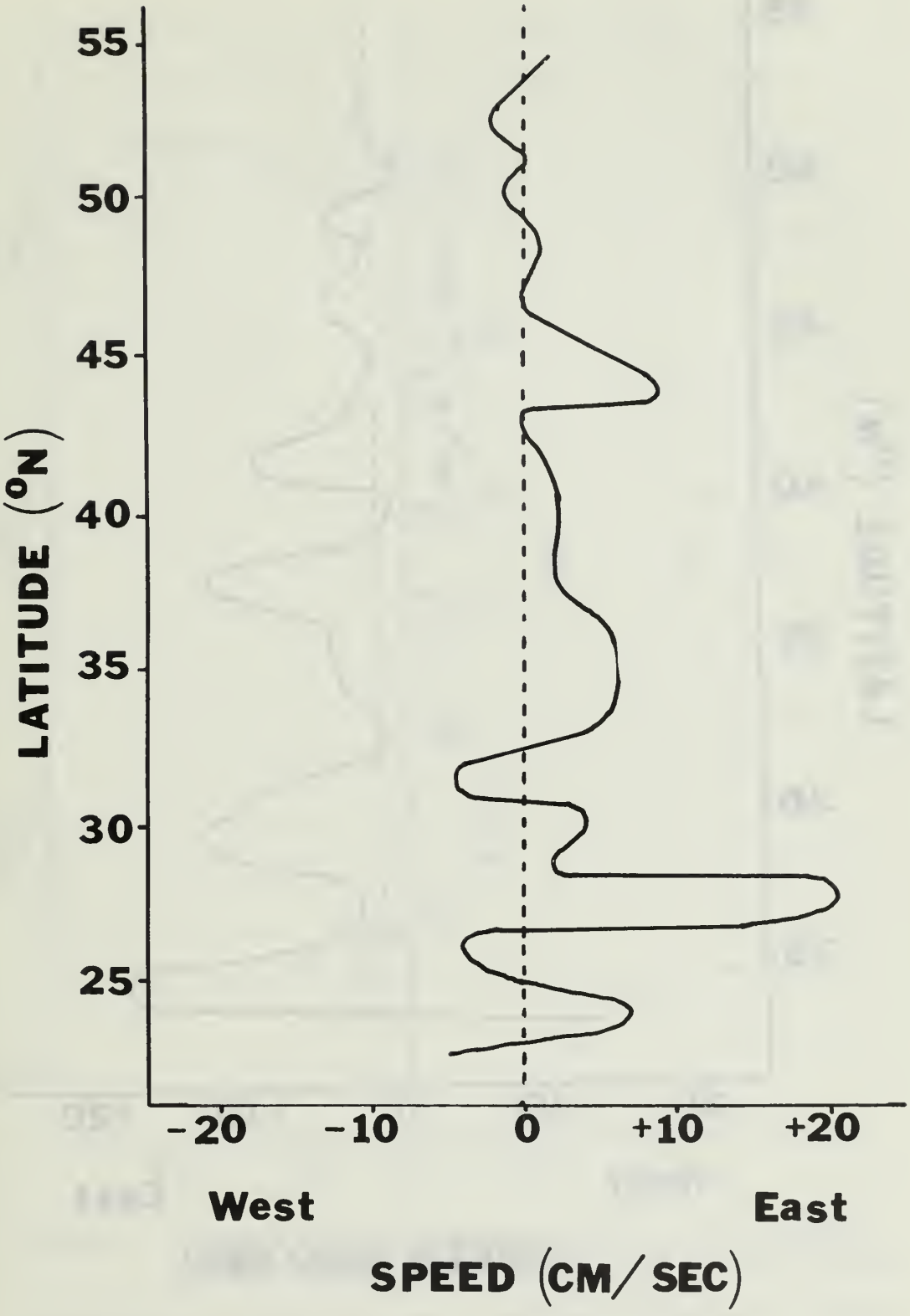

Figure 6. Latitudinal variation of geostrophic flow - 4 SEPT 1968.

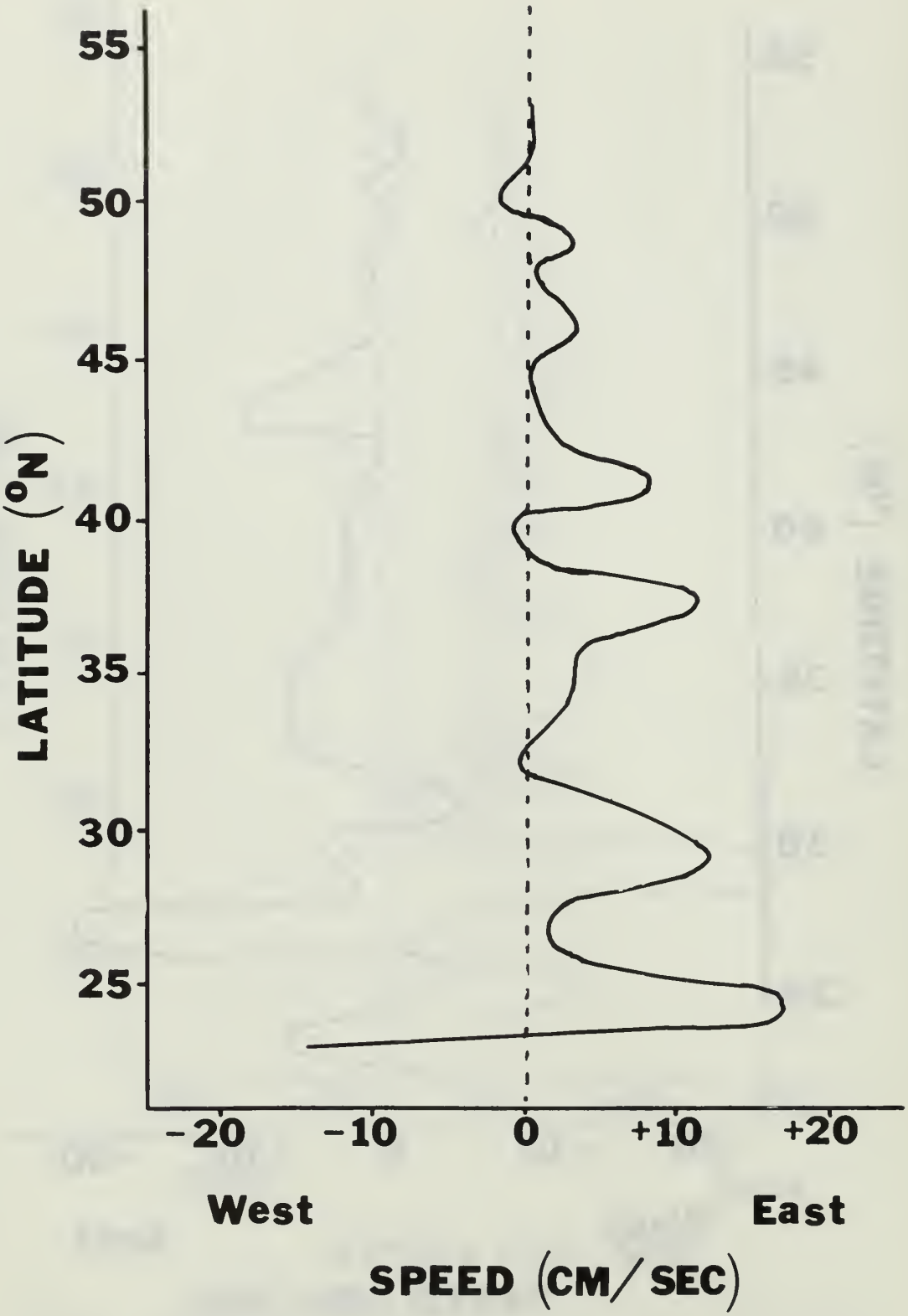

Figure 7. Latitudinal variation of geo trophic flow - 23 NOV 1968.

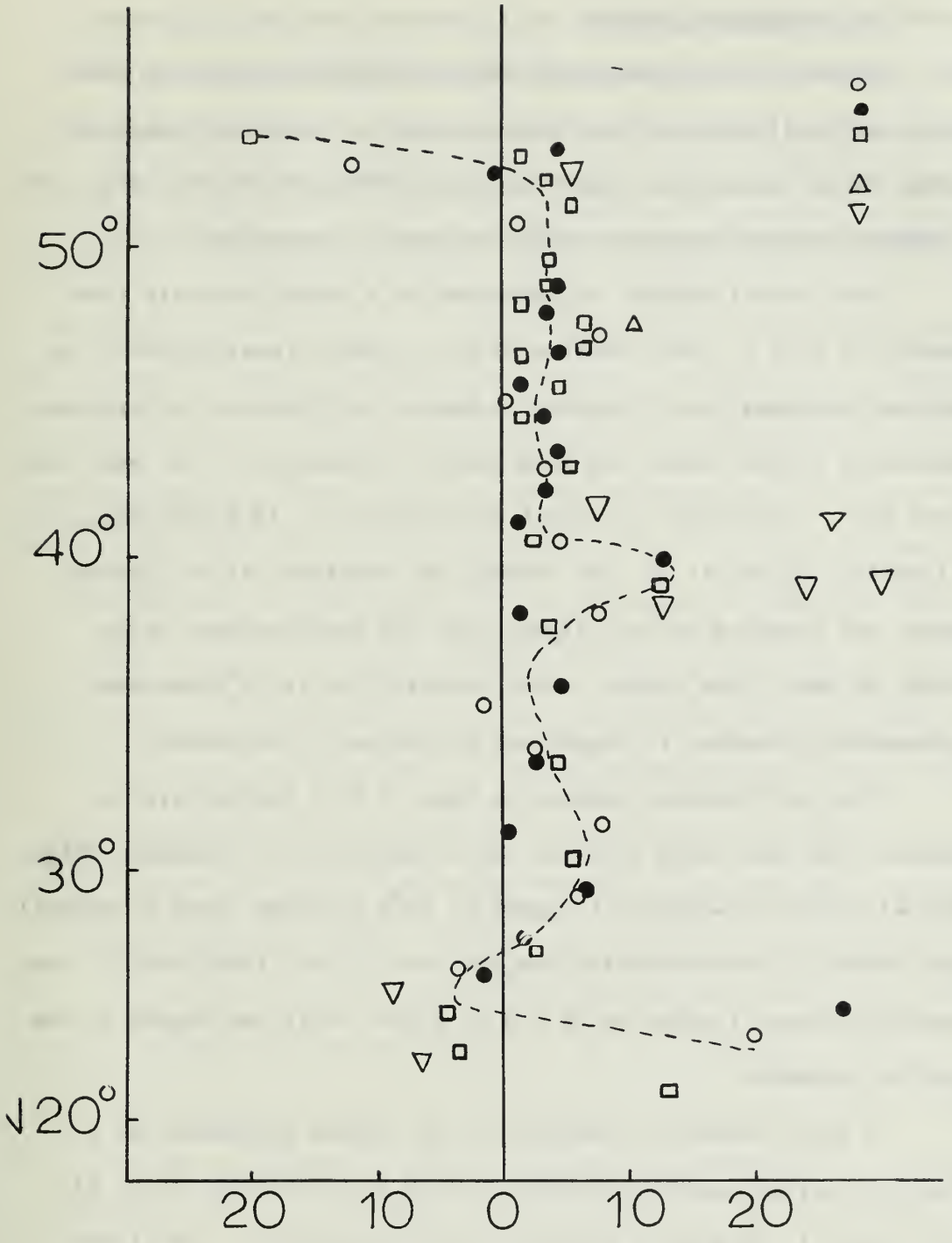

Figure 8. Comparison of calculated geostrophic surface currents versus direct measurements (After Reed and Laird, 1966).

1. In the Heating Season

Figures 3-6 represent the surface currents across the track during the final weeks of the heating season. In the mid-latitudes, between 33-52°N, the flow appears generally weak and to the east. The strongest currents occur below 33°N and vary in direction.

The overall pattern is dominated by a strong easterly flow centered at 27.7°N. The location of this current remains fixed; the magnitude averages about 14cm/sec in August and 20cm/sec in September. Immediately to the south, the flow pattern alternates to the west then to the east. The westerly current is strongest on 19 August (Fig. 3) at 15cm/sec located at 25.4°N. During the remainder of the heating season, the location varies slightly but the speed reduces to an average of about five cm/sec. The easterly flow at 24°N averages approximately 14cm/sec in August and six cm/sec in September.

The most variable feature in Figs. 3-6 is the pattern of westerly flow just north of 29°N. On 19 August and 2 September (Figs. 2 and 4) there are westerly toungues at 30°N (average speed 7.3cm/sec) which vanish in the succeeding two and three days. Additionally, the westerly currents located at 32.4°N in August shift one degree to the south by September.

A final feature of interest is the sudden appearance of a relatively strong eastward current at 44°N on 4 September (Fig. 6). This current is marginally present in previous figures, and either disappears or moves south by November.

2. In the Cooling Season

Figure 7 presents the velocity field after about two months of cooling. Not unexpectedly, the pattern has changed considerably.

The only significant westward flow is in the extreme south; the weak westward flow persists at 50°N. Along the remainder of the track, eastward movement has intensified, developing fairly strong currents at 24, 29, 37, and 41°N latitude. This corresponds to the general eastward drift characteristic of the central subarctic Pacific.

IV. THERMAL STRUCTURE ALONG 158°W LONGITUDE

Thermal structure can be defined as the relationship between temperature and depth as a function of time and space. In this context, the five AXBT sections are particularly adaptable to an investigation of thermal structure. There are, of course, several descriptive parameters and analytic techniques available to describe structure; two have been chosen to present the AXBT data. The first and most straightforward is to plot selected isopleths of temperature (isotherms) along each section. The second is to show the spacial variation of the thermocline by plotting calculated depths to the top (Z_t), center (Z_c) and bottom (Z_b) of the thermocline versus latitude.

The definition and determination of the Z-parameters follows Boston (1966). Boston's method of analysis is essentially a curve-fitting technique making use of some fundamental statistical theorems. He introduced the notion of a "Gaussian Thermocline", developed expressions for associated parameters, and illustrated the application of these parameters to non-Gaussian distributions.

Z_t and Z_b, defined in terms of Z_c, approximate the depths to the upper and lower limits of a layer of water with a large temperature gradient. The fundamental parameter is Z_c. To define Z_c it is necessary to introduce a function Z(T) which describes a distribution of depths as a function of temperature. This distribution is developed from original data by forming an ordered set of depths, beginning at the surface, corresponding to temperatures separated by a constant increment. Z_c is then defined as the depth corresponding to the point of inflection

in the distribution function Z(T). Details of the method are summarized briefly in the following sections.

A. THE GAUSSIAN THERMOCLINE

A Gaussian thermocline is defined by a distribution of temperature as a function of depth, T(Z), whose frequency function (i.e. whose first derivative) forms a normal or Gaussian curve. Characteristic of a Gaussian curve is symmetry about the first moment and symmetrically located points of inflection and points of maximum rate of change. Making use of these features, Boston demonstrated that Z_c corresponds to the first moment ($\bar{Z}$) and that Z_t and Z_b correspond to points of maximum rate of change ($\bar{Z} \pm \sqrt{3}S$), where S is standard deviation. Implicit in this development is a normalized temperature field in which successively decreasing values of temperature are associated uniquely with increasing depths (i.e. the distribution functions T(Z) and Z(T) are coincident).

Grosfils (1968) has developed numerical methods for analyzing a Gaussian thermocline by digital computor. The requisite inputs are the surface and bottom temperatures and depths read at a constant temperature interval. Basically, the technique is to compute the first and second moments of the frequency function which define mean ($\bar{Z}$) and variance (S^2) respectively. He points out, however, that the error inherent in transforming from integrals to summations to compute moments is closely related to the temperature increment chosen to define the depth vector. The error is most apparent in the value of standard deviation (S) developed from the second moment; therefore, he introduced a weight factor K which varies as the temperature increment. This

results in the following expressions for the Z-parameters (Z decreases with depth):

$$Z_c = \bar{Z} \tag{7}$$

$$Z_t = Z_c + K(S) \tag{8}$$

$$Z_b = Z_c - K(S) \tag{9}$$

Typical values of K are 1.47 and 1.30 for temperature increments of 0.5 and 1.0 degree respectively.

1. Non-Gaussian Distributions

The technique summarized above may be applied to non-Gaussian distributions by first recalling the definition of Z_c presented at the beginning of this section. As noted, the original data must be re-structured to define a distribution function Z(T) - the ordered array of depths read at a constant temperature interval. Once this is done, Z_c is determined by straightforward finite-difference operations on Z(T). Z_c corresponds to the depth at which the second finite difference passes through zero.

With Z_c determined, the procedure is to consider separately the segments of the distribution curve lying above and below Z_c. For convenience, let the functions F and G represent the two segments such that F is defined for $Z \leq Z_c$ and conversely for G. At this point an artifice is introduced whereby each of the functions F and G are supplied with a "tail" (to be graphic if not exactly precise) fashioned so as to transform F and G into Gaussian Thermoclines. Standard deviations (S_f and S_g) for each distribution are then calculated and substituted into equations (8) and (9), S_f defining Z_t and S_g defining Z_b.

2. Application to AXBT Data

In the analysis of the AXBT data, the temperature distribution was assumed to be non-Gaussian in those traces with one major thermocline. In the case of well-defined multiple thermoclines, the Z-parameters were calculated for the most shallow, assuming a Gaussian distribution. Temperature inversions were neglected.

This somewhat cavalier treatment of multiple structure does not imply such features were considered unimportant. To the contrary, they merit a much more rigorous examination than the scope of this thesis permits.

B. LATITUDINAL VARIATION OF THE THERMOCLINE

Figures 9-13 show the variation of the top, center and bottom of the thermocline with latitude for each of the five sections. Again, the seasonal difference in gross features is most apparent. Figures 9-12 represent conditions at the end of the heating season and Fig. 13 represents conditions after about two months of cooling.

The dominant feature in August and September is the "dome" in all curves in the mid-latitudes. By November, this dome has been replaced by a distinct "dip" at about 40^{o}N latitude. The explanation for these gross features in the absence of definitive climatic and salinity data is speculative; however, the features are not inconsistent with the seasonal mixing processes characteristic of the subtropic and subarctic regions of the North Pacific (Tully, 1964). In the subtropic region, evaporation-driven convective mixing is predominant throughout the year. In the subarctic region, where precipitation exceeds evaporation, the mixing process differs in the heating and cooling seasons. During the

heating season, a near-surface halocline created by excess precipitation prevents convective mixing so that the mixed layer is primarily a function of wind speed (Tully, 1964). As the water cools, however, temperature-driven convection occurs despite the excess precipitation. Keeping these mechanisms in mind, it appears possible that the dome present in Figs. 9-12 corresponds to a transition area between the two regions wherein evaporation and precipitation are roughly in balance and and the mixing is due to wind alone. By November (Fig. 13) convective mixing has overcome the restraining influence of the seasonal halocline north of 40^{o}N latitude. The location of the dip in Fig. 13 corresponds closely with the southern boundary of the subarctic region defined by Tully. The dip suggests that the intensity of the gryral circulations characteristic of the subtropic and subarctic regions have intensified to form a convergence zone at the boundary, thus accelerating the downward mixing.

Smaller-scale features are more difficult to discern with any certainty. As nearly synoptic as the sections are, the fact remains that the observations for a given transit were not simultaneous; thus, both space and time effects are present in the data. Further, the spacing between observations was such that scales on the order of a few miles are nothing more than noise imposed on scales on the order of hundreds of miles (i.e. approximately ten times the station spacing). Features most likely to evince these constraints would be something on the order of large thermal fronts. A thermal front in the ocean is loosely defined here as a region of steep horizontal temperature gradient; the front may occur at the surface or below. A more quantitative definition is difficult in view of the wide range of intensities assigned

to thermal fronts in the literature. Knauss (1957), for example, describes a front in the equatorial Pacific where the temperature changed $3^{o}C$ in a horizontal distance of less than 100m. The more general case, however, is usually less dramatic. For any given front, the causitive forces are not always apparent; however, the presence of a front is usually reflected in a marked change in the spacial distribution of thermal parameters.

Excessive smoothing of the results of the Z-parameter calculations would tend to mask the "discontinuities" or step-like pattern associated with oceanic frontal systems. Therefore, the development of Figs. 9-13 was more subjective than mathematical; that is, envelopes fitted about points rather than least-square curves were examined. Because of this dependence on personal interpretation, the scatter diagrams from which Figs. 9-13 were developed are included as Appendix A.

1. In the Heating Season

In addition to the dome already mentioned, another feature that appears regularly during the heating season is the slight upward trend in all curves just north of $50^{o}N$ latitude. The hazzards of speculating about current effects based solely on the geostrophic component are appreciated; however, it is interesting to note that the upward trend corresponds to the location of the weak westward flow noted in the velocity patterns. The implication, as stated earlier, is that the westward flow results from a convergence of the Alaska stream and the subarctic current; that is, the Alaska gyre extends at least as far west as $158^{o}W$ longitude.

More specific details of thermocline variation and the relation to surface flow during the heating season are presented below.

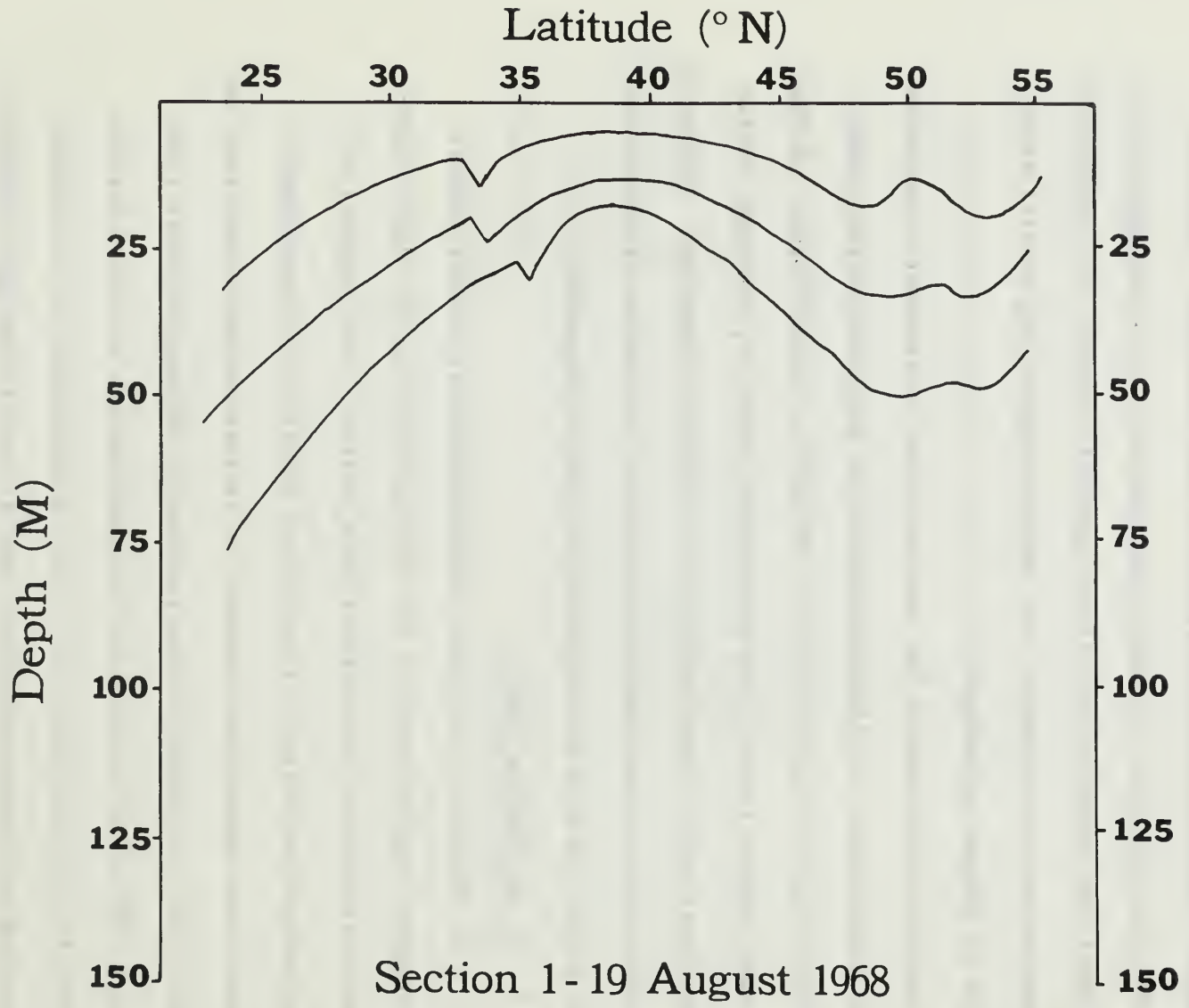

Figure 9. Latitudinal variation of the thermocline - 19 AUG 1968.

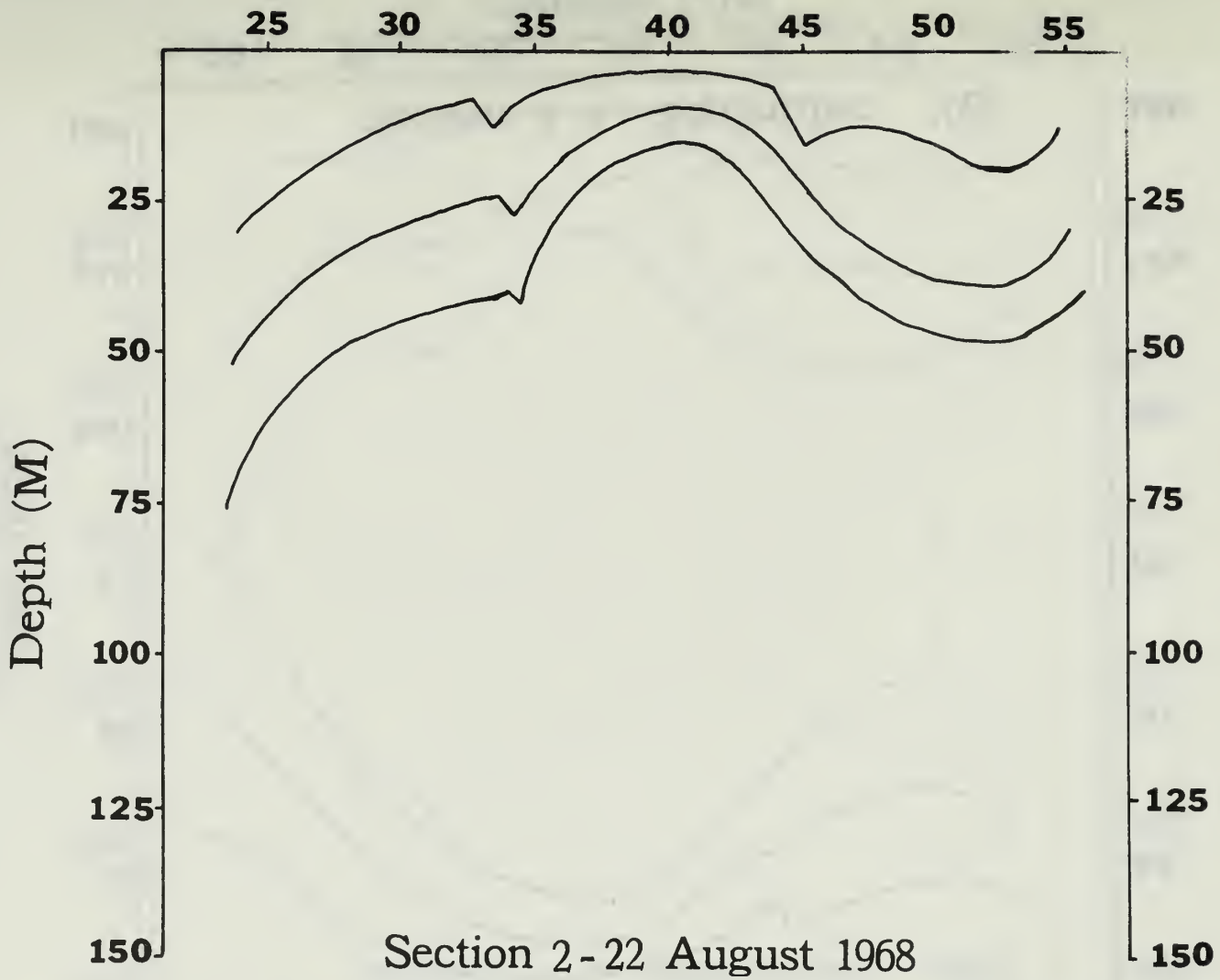

Figure 10. Latitudinal variation of the thermocline - 22 AUG 1968.

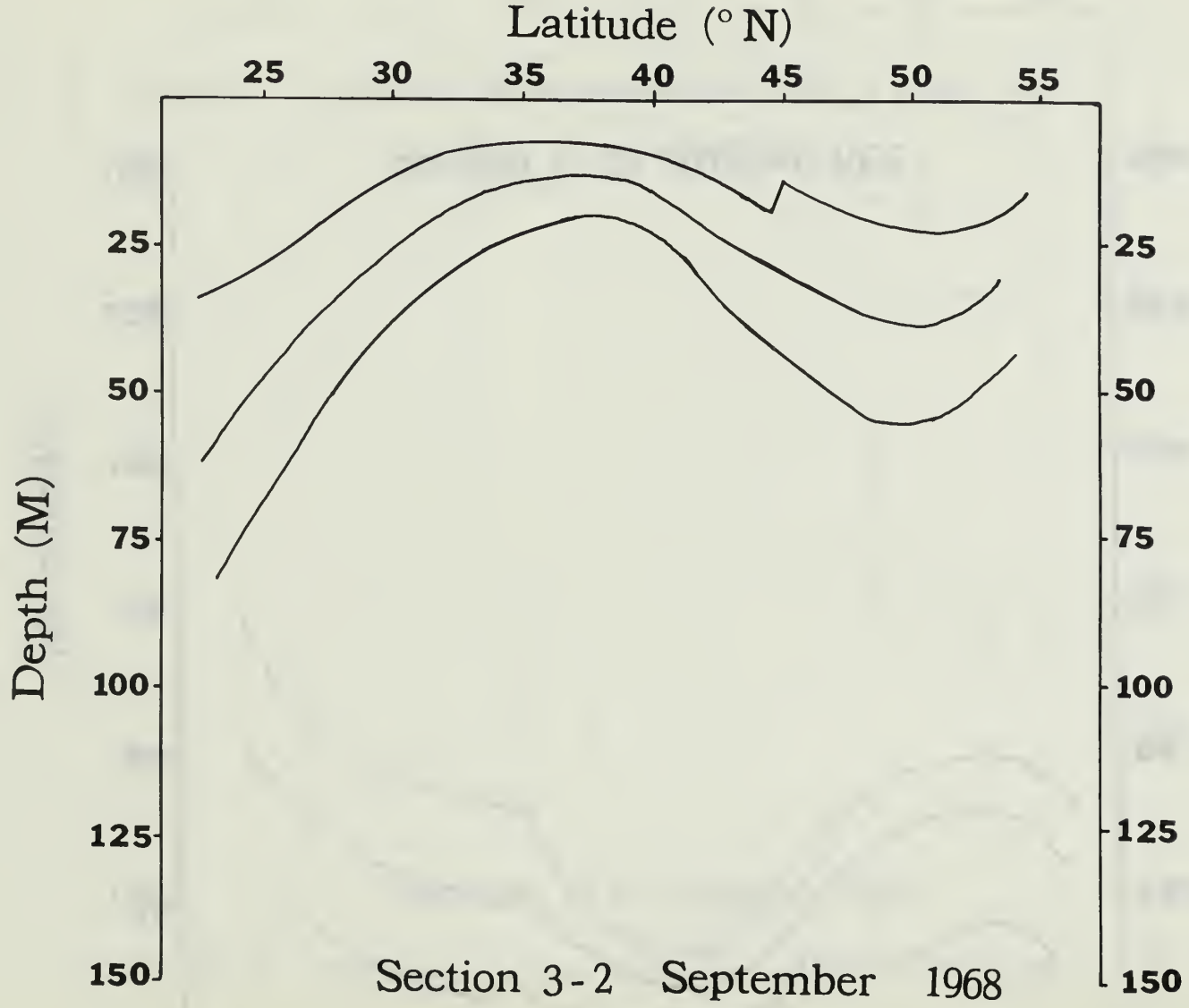

Figure 11. Latitudinal variation of the thermocline - 2 SEPT 1968

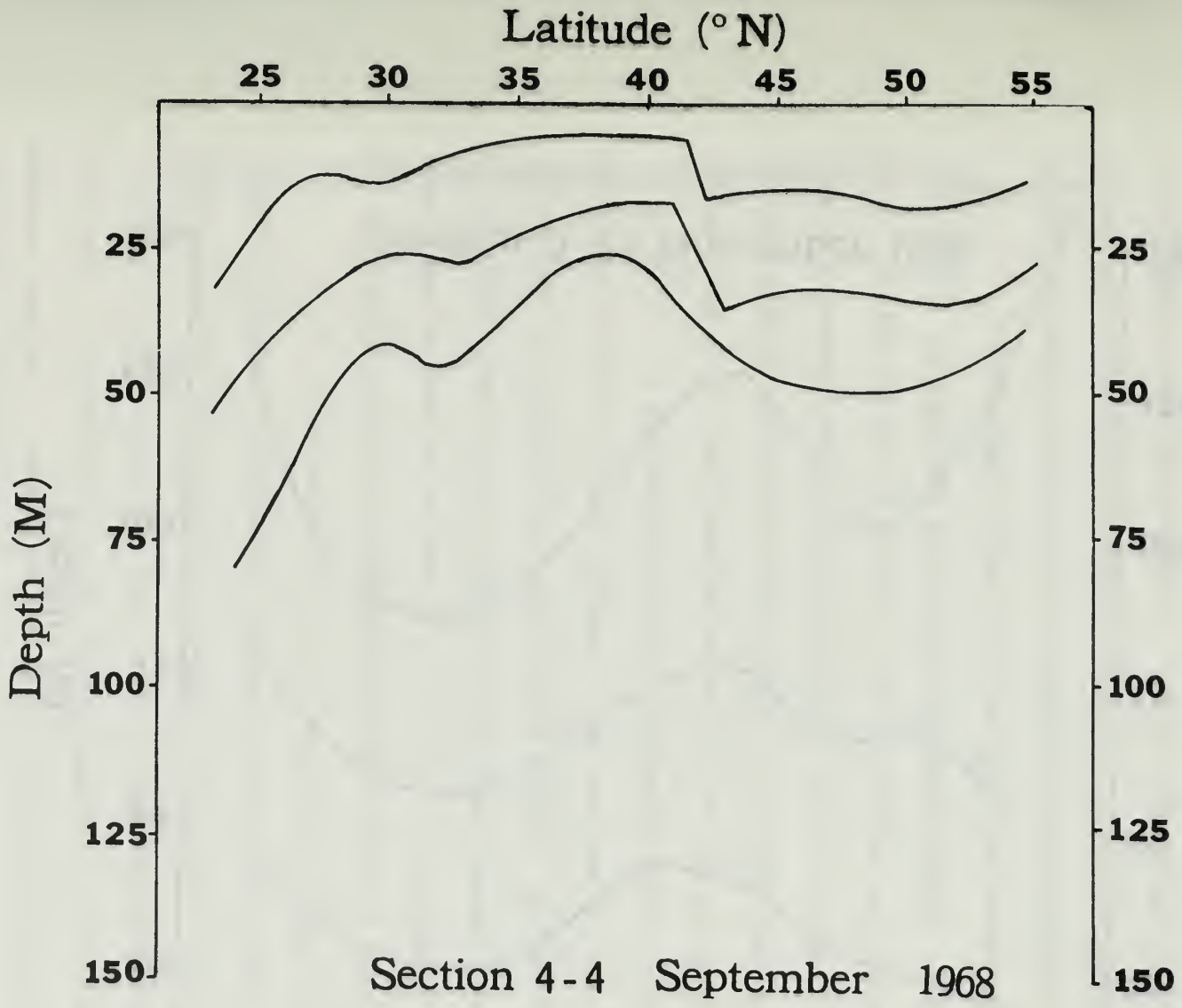

Figure 12. Latitudinal variation of the thermocline - 4 SEPT 1968.

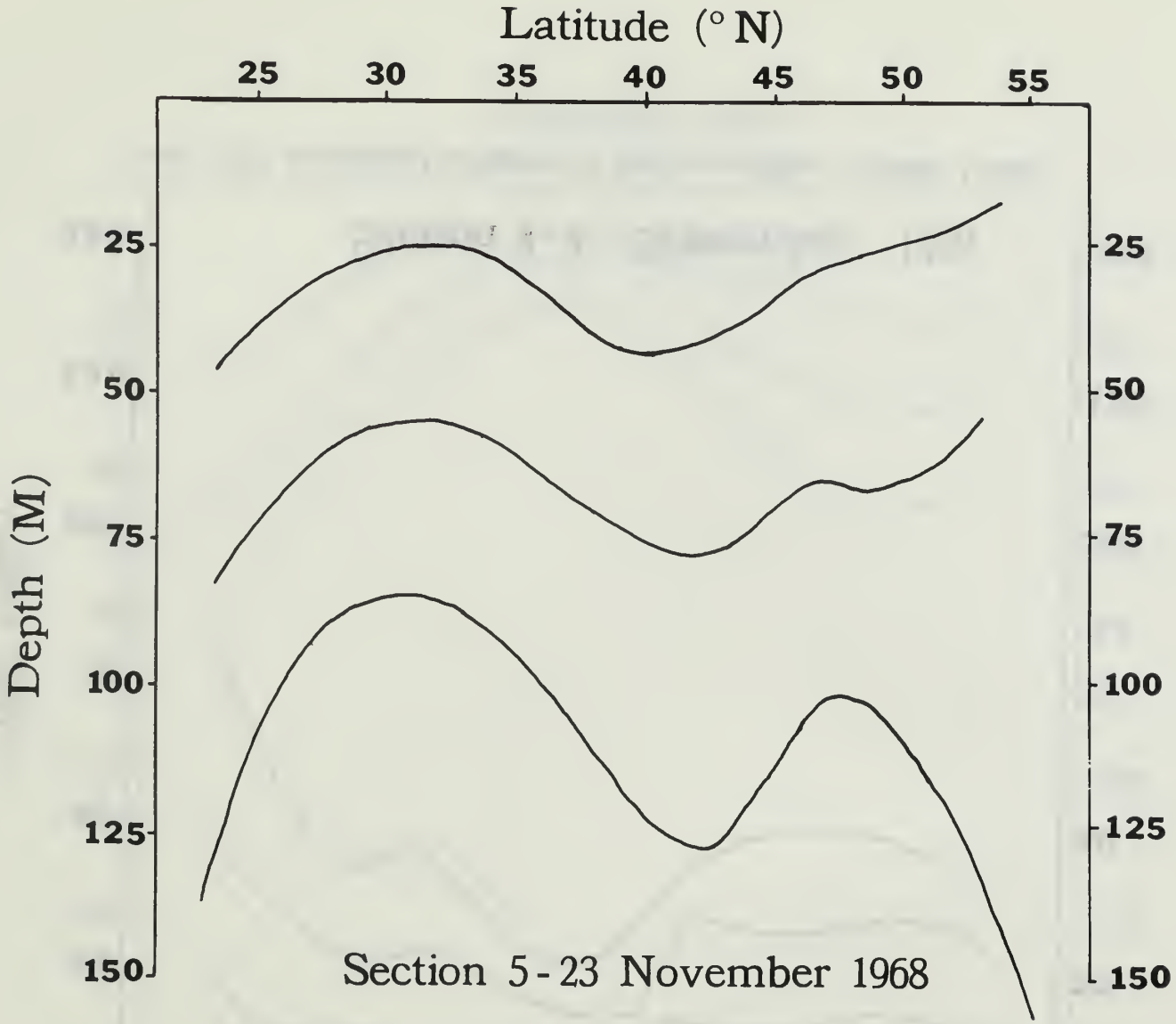

Figure 13. Latitudinal variation of the thermocline - 23 NOV 1968.

a. 19 August (Fig. 9). The dome structure extends between 35-45°N. The vertical extent of the thermocline is smallest in this area - on the order of 15m. Fronts appear in the top and center curves at 33°N and in the bottom at 35°N. The top and center frontal zones correspond to the shear in current indicated in Fig. 3; however, other strong shear flows have no apparent effect on the thermocline.

b. 22 August (Fig. 10). The upper and center fronts at 33°N remain, although the center has deepened slightly. The bottom front, however, has deepened about 18m and shifted one degree to the south. A current shear is again located at 33°N. An additional front has developed in the upper curve at 45°N; in the same time period, the surface current at that location decreased from four cm/sec to zero.

c. 2 September (Fig. 11). The upper front remains at 45°N; all other frontal zones have vanished. The dome has shifted to the south about five degrees and appears quite smooth. The vertical extent of the thermocline is still smallest in the dome; however, the entire feature has deepened about four meters. There is no apparent correlation between surface currents and thermal structure anywhere along the track.

d. 4 September (Fig. 12). The gross features along the track are similar to preceeding sections; however, the change in detail developed in two days is quite pronounced. The dome structure has thickened to about 25m and a "kink" or secondary dome has developed in the south. This contrasts to the smooth appearance of the dome in previous sections. Fronts have formed in the top and center curves at 42°N; the center front is quite steep and corresponds roughly to the sudden increase in the eastward current observed in Fig. 6. These sudden changes, particularly south of 30°N, lead one to suspect

increased atmospheric effects at the surface, possibly high winds or rain.

2. In the Cooling Season

Figure 13 indicates that the seasonal thermocline has all but disintegrated and is sinking to the level of the permanent thermocline. This deterioration is accompanied by a general increase in eastward flow between 25-50°N. As noted earlier, the axis of the dip seems to correspond to the transition area between the subtropic and subarctic regions.

A large smooth "hump" has developed in all curves in the south. The hump seems unrelated to the dome noted during August and September; however, its cause is not clear. It may be the result of a Taylor column effect to be discussed in the next section.

C. LATITUDINAL VARIATION OF ISOTHERMAL LINES

Figures 14-18 present the pattern of isotherms along the five sections together with the traces from which they were developed. Unfortunately, the scale of the figures eliminate much of the finer detail, particularly in the surface layer. However, variations noted in the thermocline parameters appear to be consistent with the near-surface isotherm patterns when examined on larger-scale graphics.

One of the most prominent features of the isotherm contours is the abrupt, frontal character of the 8°-isotherm - rising some 180m in approximately 30 nautical miles. There is little variation in the location of the steepness of the front in this isotherm below about 60m. Neumann and Pierson (1966), among others, have described the 8°-isotherm as the boundary between the cold and warm spheres in the ocean. In Figs.

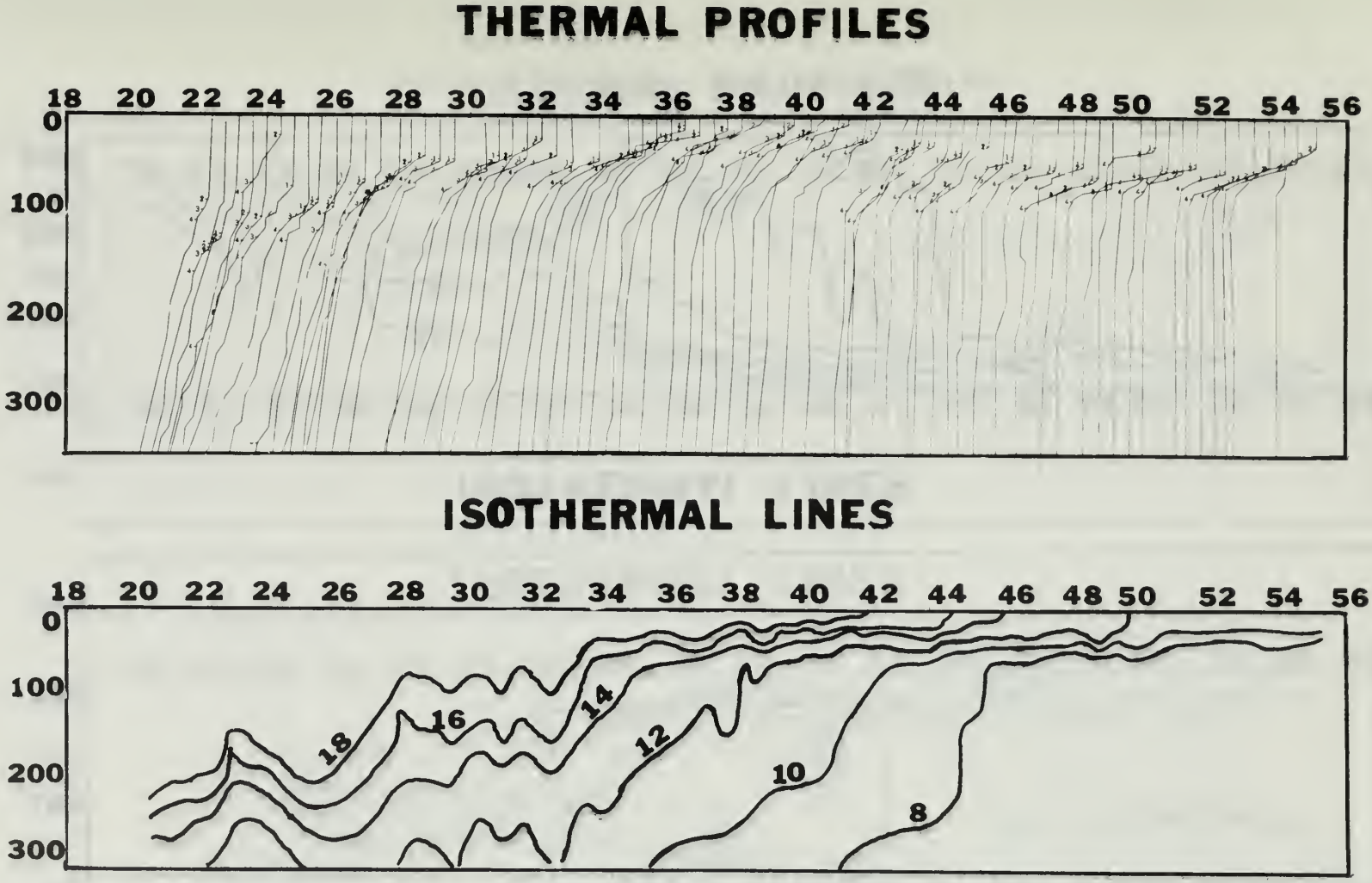

Figure 14. 19 AUGUST 1968 Thermal Sections.

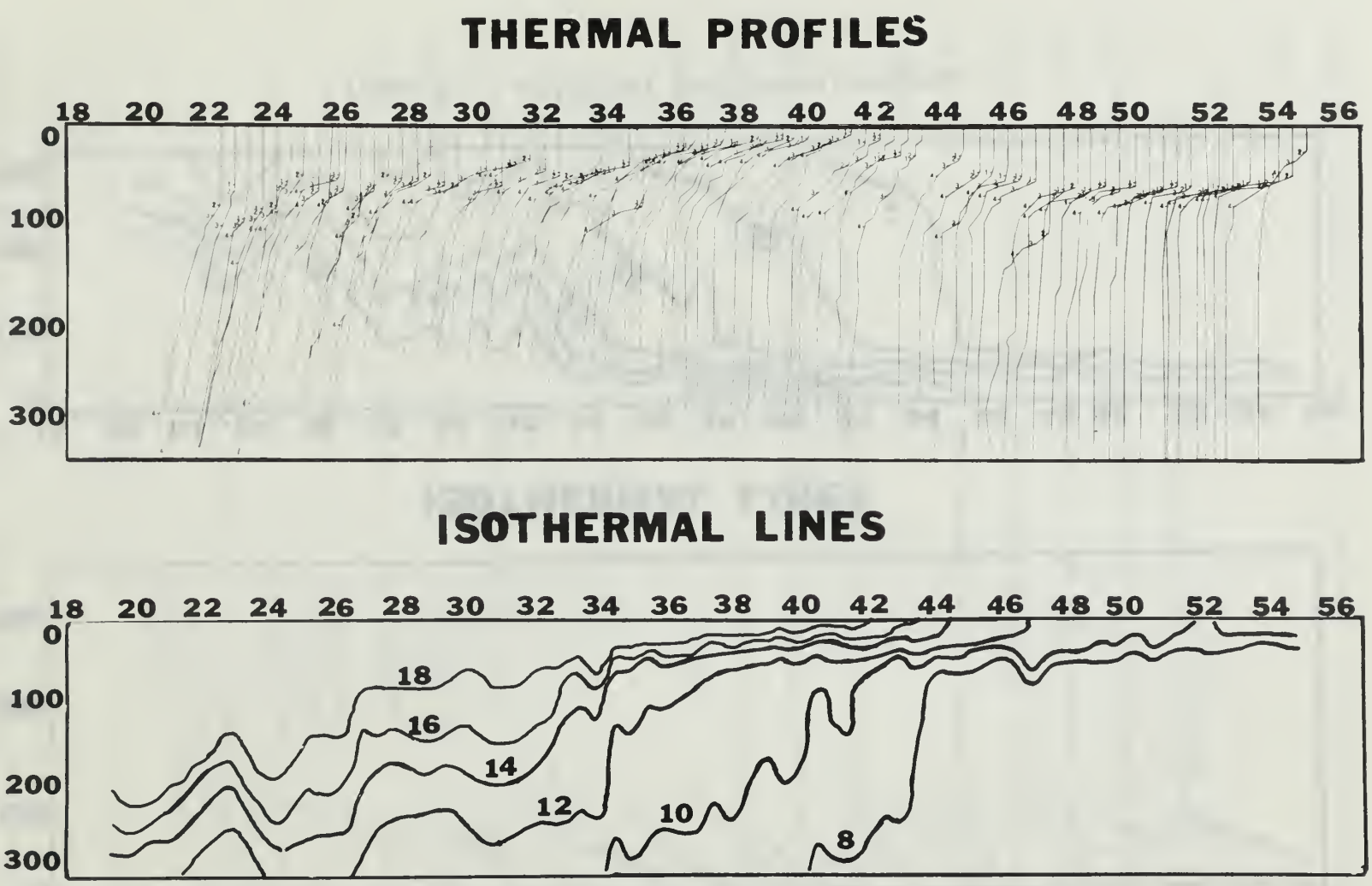

Figure 15. 22 AUGUST 1968 Thermal Sections.

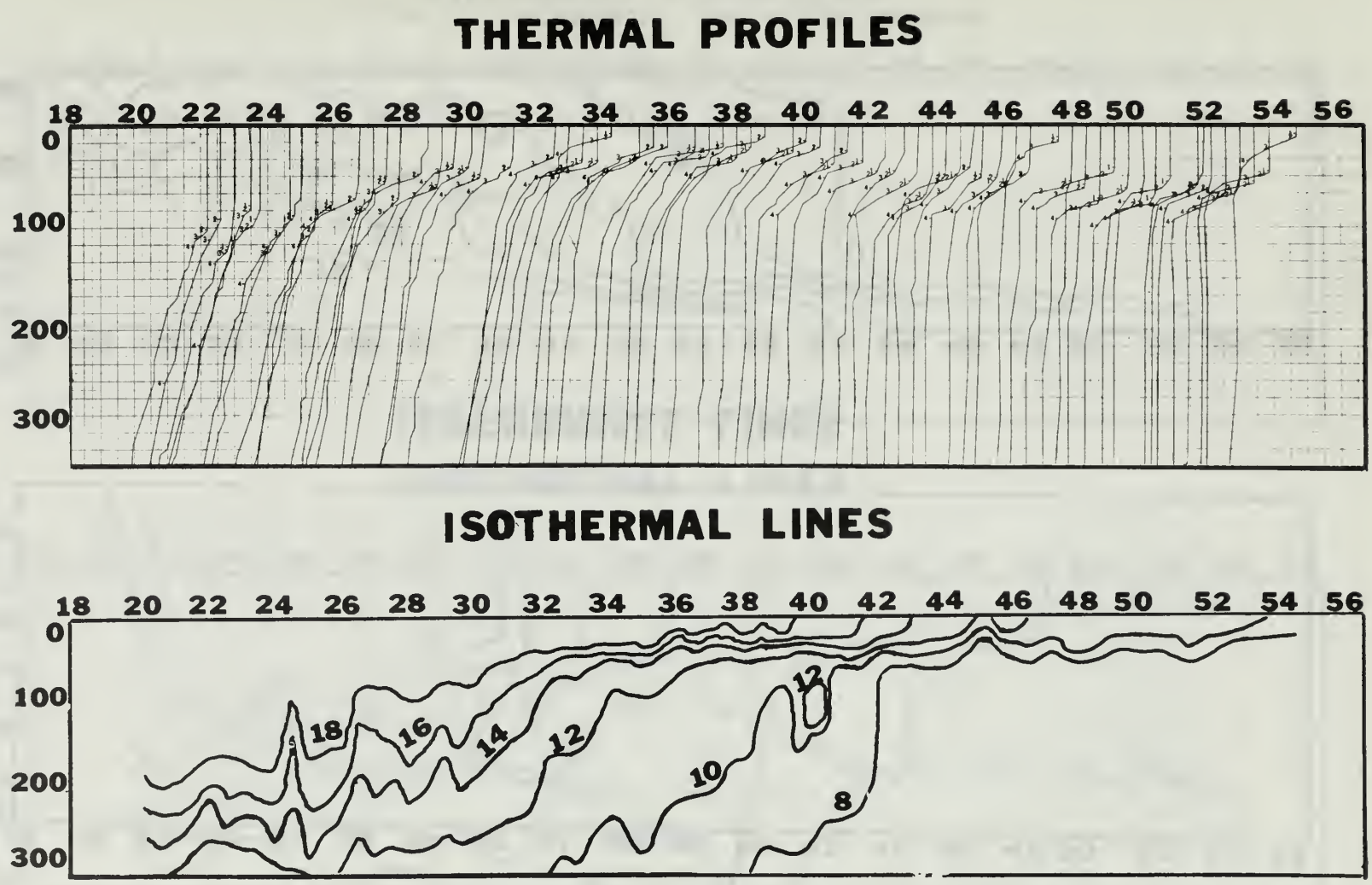

Figure 16. 2 SEPTEMBER 1968 Thermal Sections.

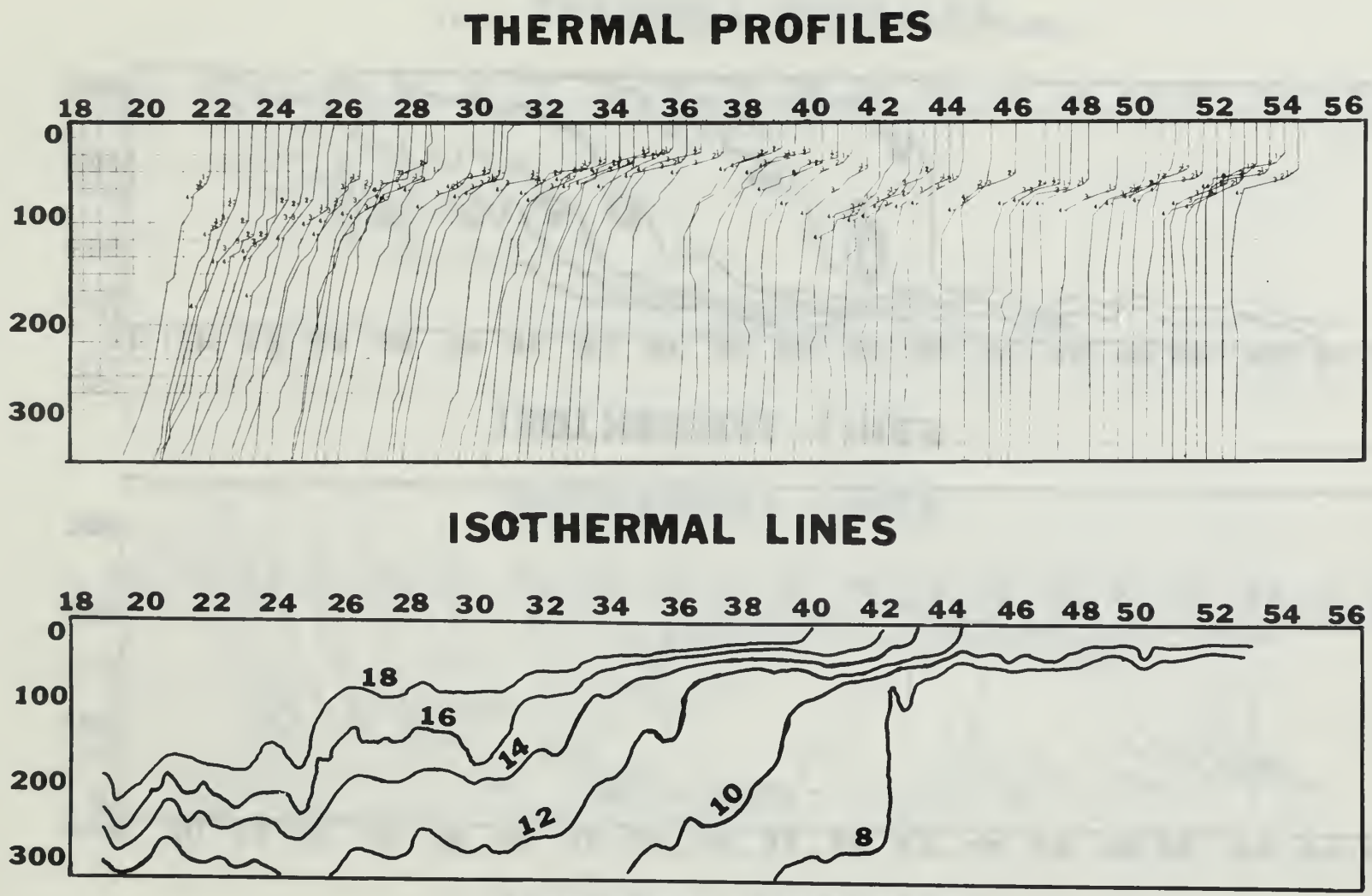

Figure 17. 4 SEPTEMBER 1968 Thermal Sections.

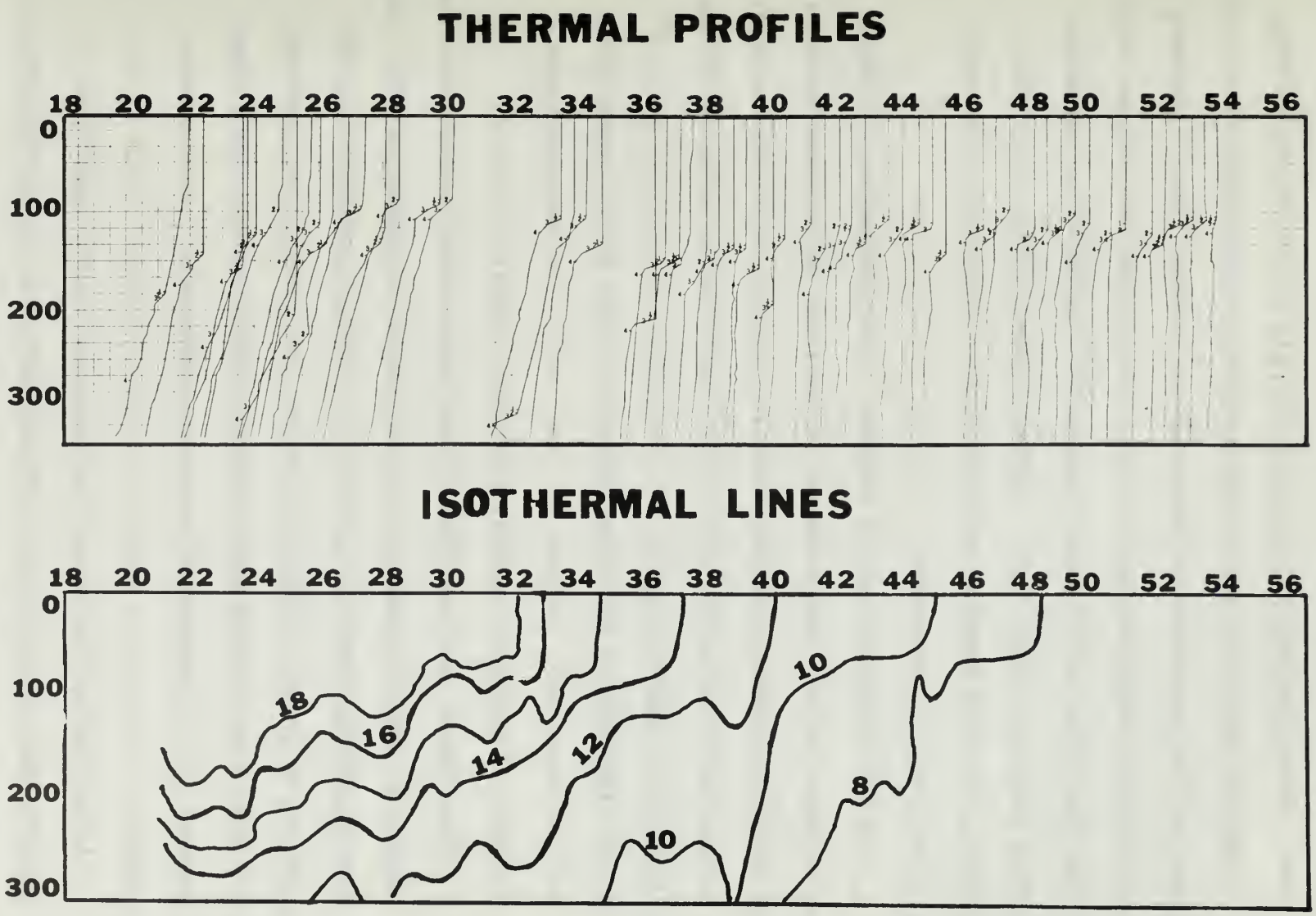

Figure 18. 23 NOVEMBER 1968 Thermal Sections.

14-18 it seems to be the index or seasonal activity in the subarctic zone. During the transition from the heating to cooling season (Figs. 17 and 18), the 8^{o}-isotherm in the surface layer has shifted southward, intersecting the surface at about 48^{o}N in November. The 6^{o}-isotherm, on the other hand, has maintained its general shape but deepened about 20m. The effect of the steep front in the 8^{o}-isotherm on the surface layer does not reflect in the figures; however, during the heating season, the front seems to mark the northern limit of the dome noted in the thermocline patterns.

The 10^{o}-isotherm generally conforms to the 8^{o}-isotherm. In overall shape, the isotherms south of (warmer than) 10^{o}C are more horizontal; from 10^{o}C and colder, the isotherms rise abruptly to the surface layer. During the heating season, the colder isotherms rise to between 20-40m and then run roughly parallel to the surface. The pattern of the 8^{o}- and 10^{o}-isotherms in August and September (Figs. 14-17), particularly north of about 48^{o}N, suggests the lower limit of an estuarine embayment such as described by Tully and Barber (1960).

The November sections (Figs. 13 and 18) indicate the transition area between the subarctic and subtropic regions to be between 41-45^{o}N. The wide separation between the 10^{o} and 12^{o} isotherms corresponds to the location of the dip in Fig. 13. Further, the shape of the isotherms 10^{o}C and colder is noticeably different than the warmer lines. This suggests the 10^{o}-isotherm as the southern boundary of the subarctic region.

In the south, the limit of the dome noted in the thermocline patterns seems to correspond to the 18^{o}-isotherm. The frontal character of this isotherm is not as intense as the 8^{o} line; however, the southern

fronts in the thermocline curves in August (Figs. 9 and 10) coincide with a marked rise in the 18°-isotherm on those dates.

The most interesting feature of the deeper thermal structure is the dome or "hump" in the isotherms between 23-26°N latitude. The mechanism generating this feature is not clear. One possibility is that it is simply an internal wave phenomenon resulting from waves either reflected or generated by the Hawaiian Islands. Amphidromic tide waves are progressive waves that can be reflected by obstacles such as the Hawaiian Islands. There is general agreement that the semidiurnal wave approaches Hawaii from the northeast. However, Wyrtki and Graefe (1967) point out disagreement as to the direction of the diurnal wave approach to Hawaii. The point is that the progression of amphidromic waves across the North Pacific is not certain, implying that the reflection of these waves is equally uncertain. Nevertheless, the possibility remains although the consistency of the dome in time and space militates strongly against such an argument.

A second possibility is that the feature is caused by a Taylor-column effect such as described by Greenspan (1968). The Taylor column was predicted theoretically by J. Proudman in 1916 and confirmed in the laboratory by G. I. Taylor in 1921. The essential feature of a Taylor column is a fluid system in a state of solid body rotation in which a fluid motion is induced relative to a fixed obstacle in the system. To illustrate, consider an object such as a hocky puck secured to the bottom of a filled container of fluid that is rotating on a turntable. By varying the rotation of the turntable slightly, a slow relative motion between the fluid and the hockey puck is established. A two-dimensional flow pattern results that is most striking.

An excellent photograph presented by Greenspan (1968, Fig. 1.2) clearly shows a cylindrical column of fluid rigidly attached to a small protuberance on the bottom of a beaker. Additional photographs demonstrate that flow about the column is much the same as if the column were an impermeable solid.

Consider now the rugged bottom topography illustrated in Fig. 1 at approximately the same latitudes in which the isotherm humps appear. The urge to infer a relation between the two features is virtually irresistable albeit speculative.

In the previous section, reference was made to a possible Taylor-column effect in connection with the appearance in southern latitudes of a large smooth hump in the thermocline patterns in November (Fig. 13). Recall that the development of this feature was coincident with the general deterioration of the thermocline. The implication is that if a Taylor-column effect does exist, it is bounded at the top by the thermocline.

Unfortunately, there is little evidence documenting the existence of Taylor columns in non-homogeneous fluid systems such as the ocean; a thorough investigation of this point is beyond the scope of this thesis. However, the consistency of the isotherm humps in time and space is sufficiently compelling to suggest that the possibility of a Taylor-column effect exists and merits further examination.

V. THE AXBT AS A SCIENTIFIC INSTRUMENT

The AXBT was developed primarily as a tactical device for use by antisubmarine warfare forces. Its purpose is to provide real-time intelligence about the shape of the temperature versus depth curve for use as input to various range prediction techniques. Hopefully, the preceeding sections have indicated the potential of the AXBT as an aid to the synoptic collection of oceanographic data. It remains to determine whether or not the data so collected can withstand the rigors of scientific analysis.

Section II outlined the operation of the AXBT. In this section the capability, reliability and accuracy of the instrument will be discussed. Statistics presented in this section were determined during an operational evaluation of the AXBT and NADC converter by the U. S. Navy (COMOPTEVFOR, 1965).

A. CAPABILITY

AXBT were launched from aircraft at altitudes from 500 to 20,000 ft. and groundspeeds from 200-360 knots. At 20,000 ft., however, complete thermograms were received from only 33% of the instruments dropped; at 10,000 ft. there was an improvement to 64%. The controling factor was the range from the aircraft to the instrument at the end of data transmission. Consequently, it was determined that altitudes and airspeeds should be selected such that the aircraft is within 30 miles of the instrument during transmission in order to receive a complete thermogram.

The NADC converter assembly is sufficiently small and light for use in helicopters. An added advantage of the system is that rotary-wing aircraft need not hover during data collection.

B. RELIABILITY

Seventy-six percent of 137 AXBT expended during the Navy tests were considered to have provided satisfactory thermograms. Most malfunctions were connected with the audio oscillator controlled by the temperature probe; common failures were abrupt frequency shifts, early termination of the signal, and weak signal.

Most malfunctions are easily recognizable by trained operators. One exception is a hung probe in isothermal water; both conditions produce similar traces.

C. ACCURACY

Accuracy of the AXBT, compared to the mechanical BT, was determined during five separate tests with a total of 84 AXBT. The airborne instruments were dropped within 500yd of an oceanographic research ship. Mechanical thermograms were obtained by the surface ship simultaneously with the airborne where practicable, but in no case was the comparison BT more than one-half hour old. The airborne thermograms were those displayed by the NADC converter assembly.

A total of 1,141 data points from the airborne thermograms were compared to the reference data. The mean algebraic error was $0.032^{\circ}F$ with a standard deviation of $1.039^{\circ}F$. The mean absolute error was $0.581^{\circ}F$ with a standard deviation of $0.861^{\circ}F$. These figures reflect contributions from the AXBT and the NADC converter as well as possible errors induced by time and space separation between the AXBT and the reference. The magnitude of each contribution is not known.

In another test, a comparison of 32 distinctive breakpoints noted on airborne thermograms with the same breakpoints from reference thermograms showed that 88% agreed within 20 ft. in depth.

D. APPLICATION

As a result of the tests described above, the AXBT was recommended for acceptance by the Navy in late 1965. The accuracy of the instrument as compared to the mechanical BT was considered satisfactory for the tactical nature of its intended use. Implicit in this acceptance by the Navy is that the AXBT enables the determination of acoustic parameters such as layer depth with sufficient accuracy and speed to maintain hot pursuit of submerged contacts.

The value of the instrument as a scientific tool depends greatly on the nature of the problem under investigation. The instrument appears to provide reasonably consistent and reliable information about relative structure (for which it was designed); however, the mean absolute error reported above ($0.581^{o}F$ or about $0.32^{o}C$) poses a serious limitation to studies requiring precise values of temperature. For example, the direction of geostrophic velocities calculated by both the dynamic and T-S gradient methods showed considerable variability when calculated for stations spaced about 50km apart; the variability decreased with increased separation. The implication is that the increased temperature differential lessened the effect of the error. This points to the real value of the AXBT - large-scale coverage. The AXBT and its shipborne counterpart, the XBT, represent the first true improvements in thermograph instrumentation since the introduction of the mechanical BT in 1937. Prior to the development of the expendable BT, instruments

employing electronic circuits rarely were able to utilize the best in electronic circuitry either due to prohibitive cost, bulk, or size of components. Dramatic advancements in the field of microelectronics generated by the space program served to ameliorate many of these difficulties.

Microelectronics appears to offer the best means for improving the AXBT. Assuming a sufficiently wide acceptance of the instrument to provide a broad base for amortizing the cost, the AXBT could be greatly improved by incorporating an additional thermal sensor at the surface. This should provide a more accurate sea surface reference temperature than is presently recorded by the temperature probe during the 75 seconds it remains at the surface.

The most immediate obstacles to be overcome before wide acceptance of expendable instruments by the scientific community are more subtle; they involve people and psychological reactions to the philosophy and concepts represented by the AXBT. When using the mechanical BT, meaningful results are greatly dependent on careful handling and careful calibration; calibration being affected as often as practicable. The production techniques used in the manufacture of the AXBT, however, are such that the instrument must be calibrated in the factory with no provision for field calibration. One can appreciate, then, the reluctance of the oceanographer to trust an instrument which he does not calibrate himself.

Confidence in instruments such as the AXBT and XBT can only come with time. Improved electronic production techniques involving careful application of quality control in reliability engineering should make it possible to assign a confidence figure to the performance of

each instrument (Snodgrass, 1966). The goal, of course, is to develop confidence in the instrument to the point where credibility can be assigned to temperature idiosyncracies observed even in a single trace.

VI. CONCLUSION

A. SUMMARY

The motive behind the approach to oceanic variability pursued in this thesis has been to determine the amount and reliability of information that could be determined solely from temperature data. Latitudinal distribution of thermocline depths and isothermal lines were selected for examination in order to demonstrate thermal structure variability in the most graphic form possible. Various techniques were attempted to determine thermocline depths; the quasi-statistical approach of the Gaussian thermocline produced the most satisfactory scatter diagrams and was, therefore, selected for presentation here. A cursory examination of geostrophic velocity fields was possible because of the recent introduction of the T-S gradient method.

B. CONCLUSIONS

The consistency of the data evidenced in the five space sections developed from airborne bathythermograms appears quite good. Based on the examination of these sections presented earlier, the following conclusions are offered:

1. The T-S gradient method is a viable technique for determining geostrophic velocity. It is computationally less complicated than the dynamic method and provides comparable results.

2. The definition and calculation of thermocline parameters using the notion of a Gaussian thermocline is a more rigorous and scientific approach to the problem than the plethora of arbitrary gradient methods that abound in the literature. The technique is not

restricted to thermal parameters or to Gaussian distributions. The variation with depth of any oceanographic parameter (such as salinity, dissolved oxygen, etc.) is adaptable to a similar analysis once a reasonable statistical representation is selected, for example the chi-square or student's t distributions.

3. The variation in depth to the thermocline during the heating season is characterized by a distinct dome-shaped distribution with latitude.

4. A disturbance in the water column exists between 23°N and 26°N latitude as evidenced by the persistent "hump" in the distribution of isothermal lines with latitude. The presence of a Taylor-column effect is possible.

5. Thermal fronts tend to form between 33-35°N and 43-45°N latitude during the heating season.

6. The AXBT has great potential as a scientific instrument and represents a significant step toward synoptic oceanographic data collection.

C. RECOMMENDATIONS

The PARKA data, considered in total, offer sufficient flexibility in time, space and scale to accommodate a variety of studies too numerous to itemize here. Further, the treatment of the AXBT data has been far from exhaustive. However, it is left to the reader to speculate on the full import of so large a body of data. Recommendations for further study enumerated below are restricted to those points specifically related to the development of the data as presented in this thesis. Specifically:

1. The possible existence of a Taylor-column effect in the waters just north of Hawaii suggests the need for a theoretical study of a simple two-layer model to investigate the behavior of a Taylor column in a stratified fluid. As a minimum, the study should address questions such as:

Does the column have any effect on the upper layer?

Can the column withstand an induced current profile?

Are there critical dimensions for the obstacle?

Eventually, the model should be expanded to include light stratification of the lower layer.

2. The results of geostrophic velocity calculations support the contention by Reed and Laird (1966) that station spacing is a critical parameter. Further, it is reasonable to expect optimum spacing to be a function of measurement error in determining the independent variables in the velocity equation. Accordingly, it is recommended that a study similar to that presented by Reed and Laird be conducted in order to establish optimum spacing criteria for use with the T-S gradient method.

3. It is recommended that statistical curve-fitting techniques similar to Boston's Gaussian thermocline be developed for the analysis of other oceanographic variables. In order to increase computor storage capacity, particular emphasis should be placed on determining the minimum number of statistical parameters required to reproduce a given distribution. Implicit in this recommendation is a re-examination of digitizing procedures wherein values of a selected parameter are recorded at predetermined depths; the reverse process described in Section IV may be more appropriate.

4. Finally, it is recommended that a design study be conducted to determine the feasibility of providing the AXBT with an additional thermal sensor at the surface in order to increase the reliability of the sea-surface reference temperature.

APPENDIX A

THERMOCLINE SCATTER DIAGRAMS

Figures 19-23, on the following pages, present the scatter diagrams from which figures 9 to 13 were developed. The scatter diagrams are presented solely to afford the reader an opportunity to evaluate the author's judgement in the subjective development of the curves describing the latitudinal variation of the top, center and bottom of the thermocline.

The depth scale in Figs. 19-23 is arbitrary. The scatter of points for the three z-parameters have been separated in depth for clarity; refer to figures 9-13 for approximate depths.

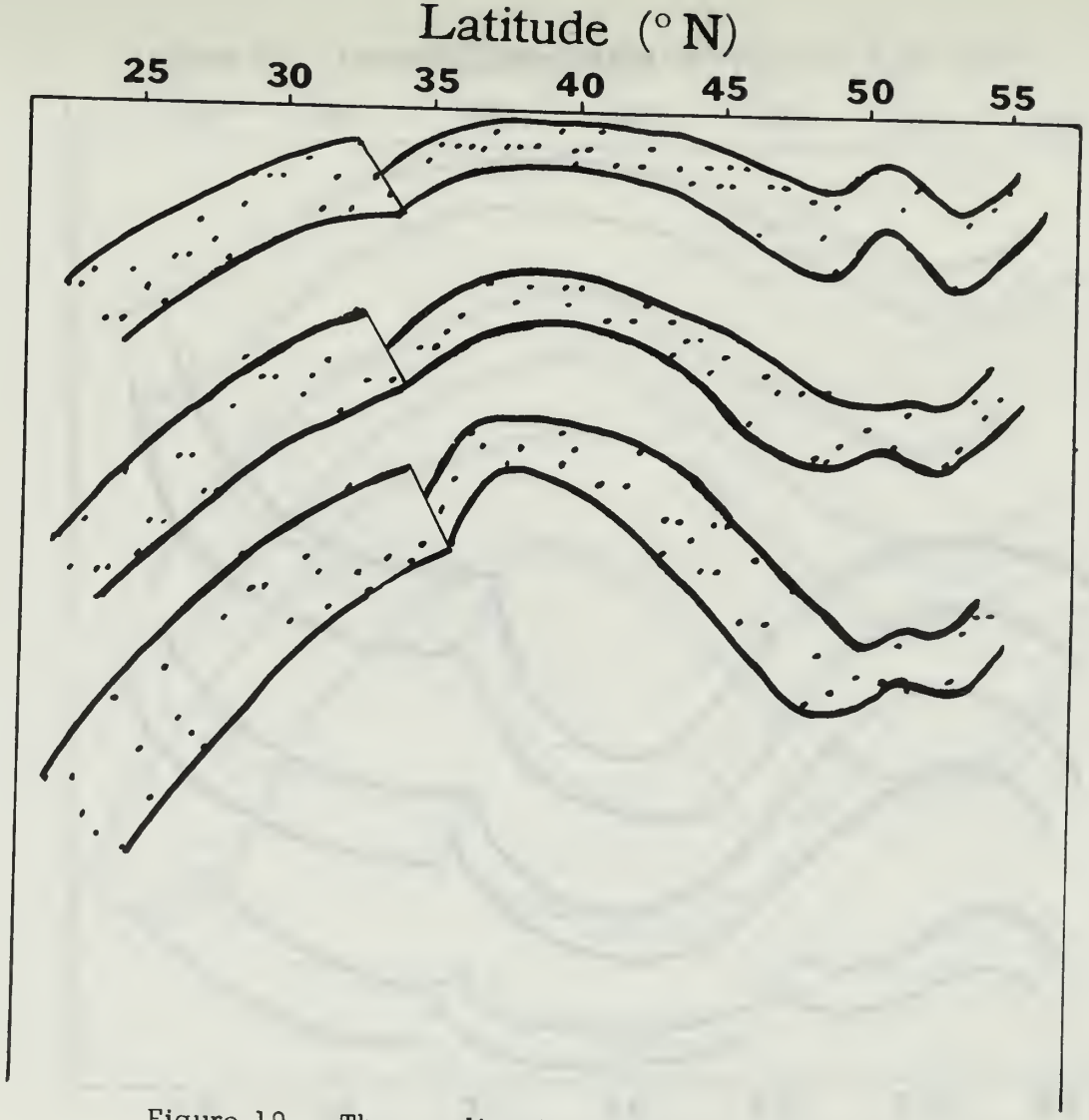

Figure 19. Thermocline Scatter Diagrams - 19 AUG 1968.

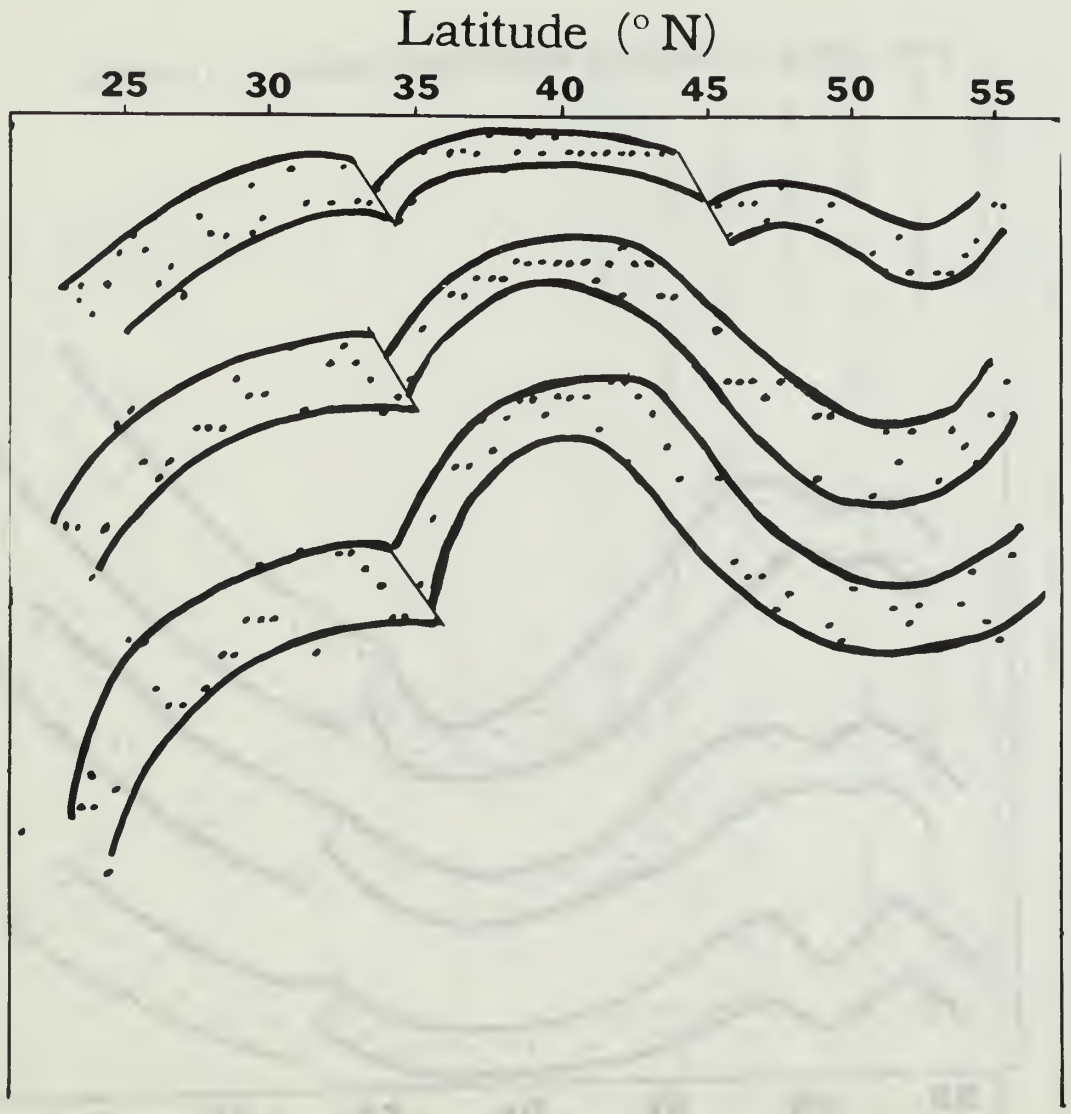

Figure 20. Thermocline Scatter Diagrams - 22 AUG 1968.

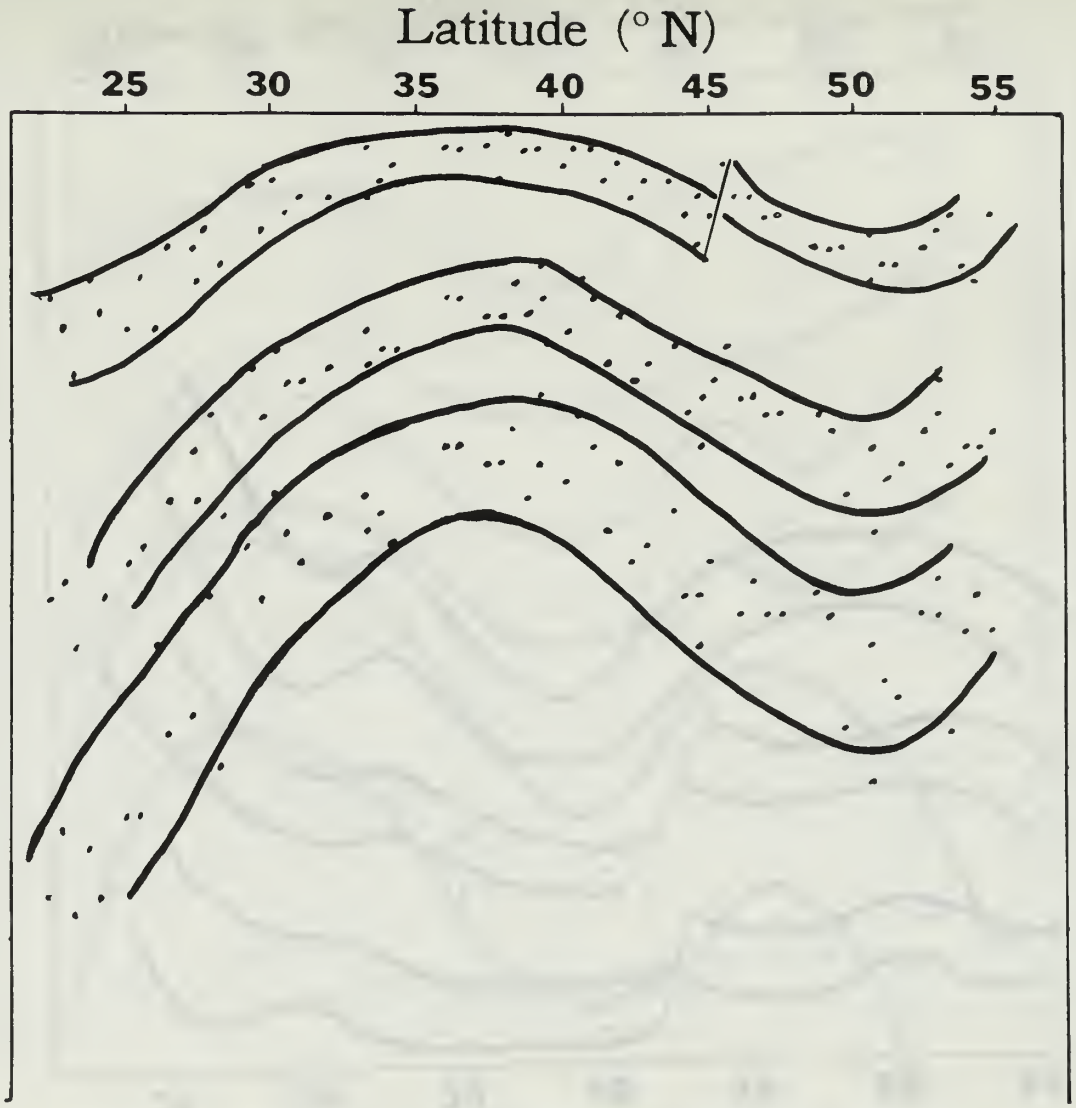

Figure 21. Thermocline Scatter Diagrams - 2 SEPT 1968.

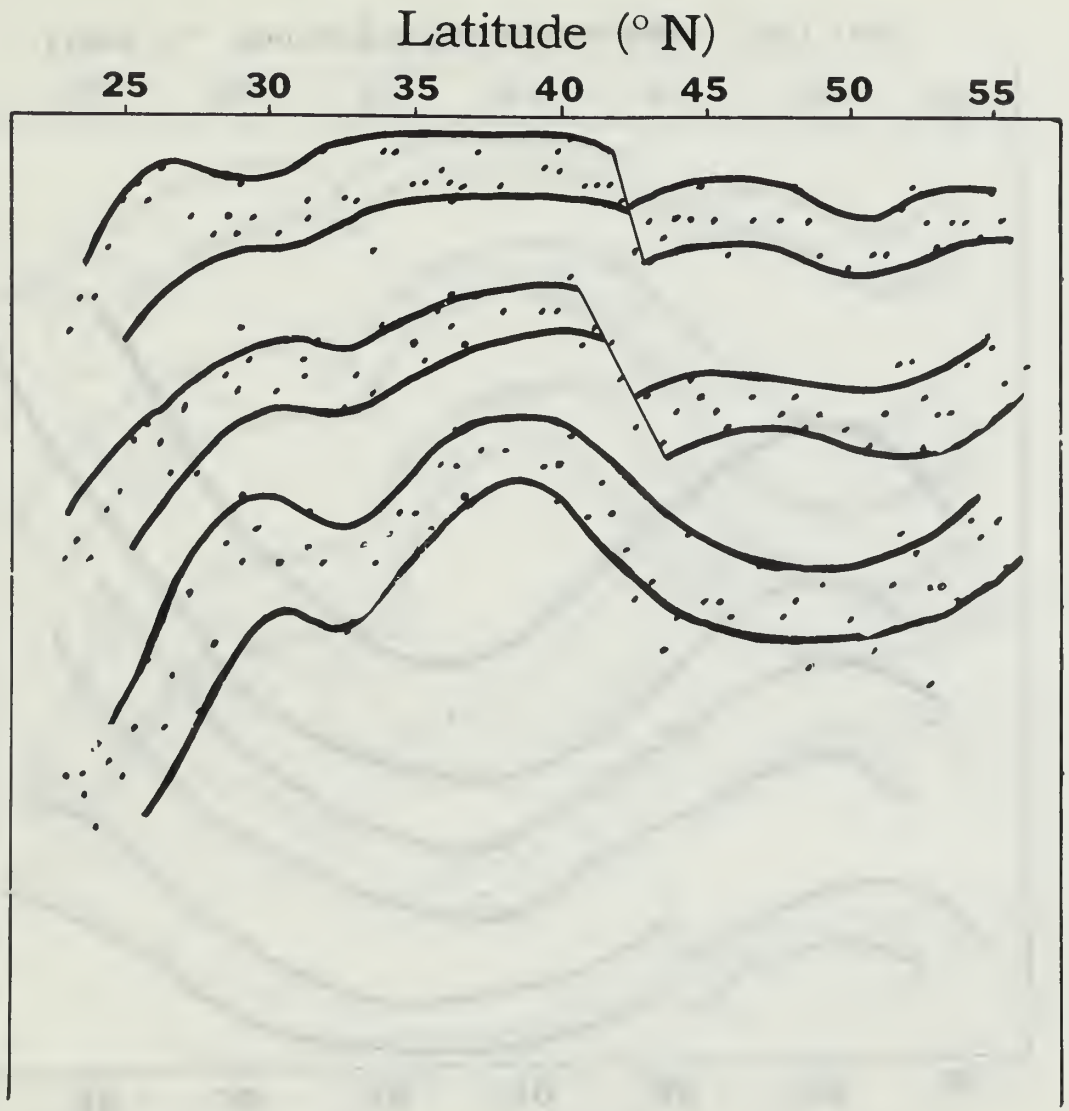

Figure 22. Thermocline Scatter Diagrams - 4 SEPT 1968.

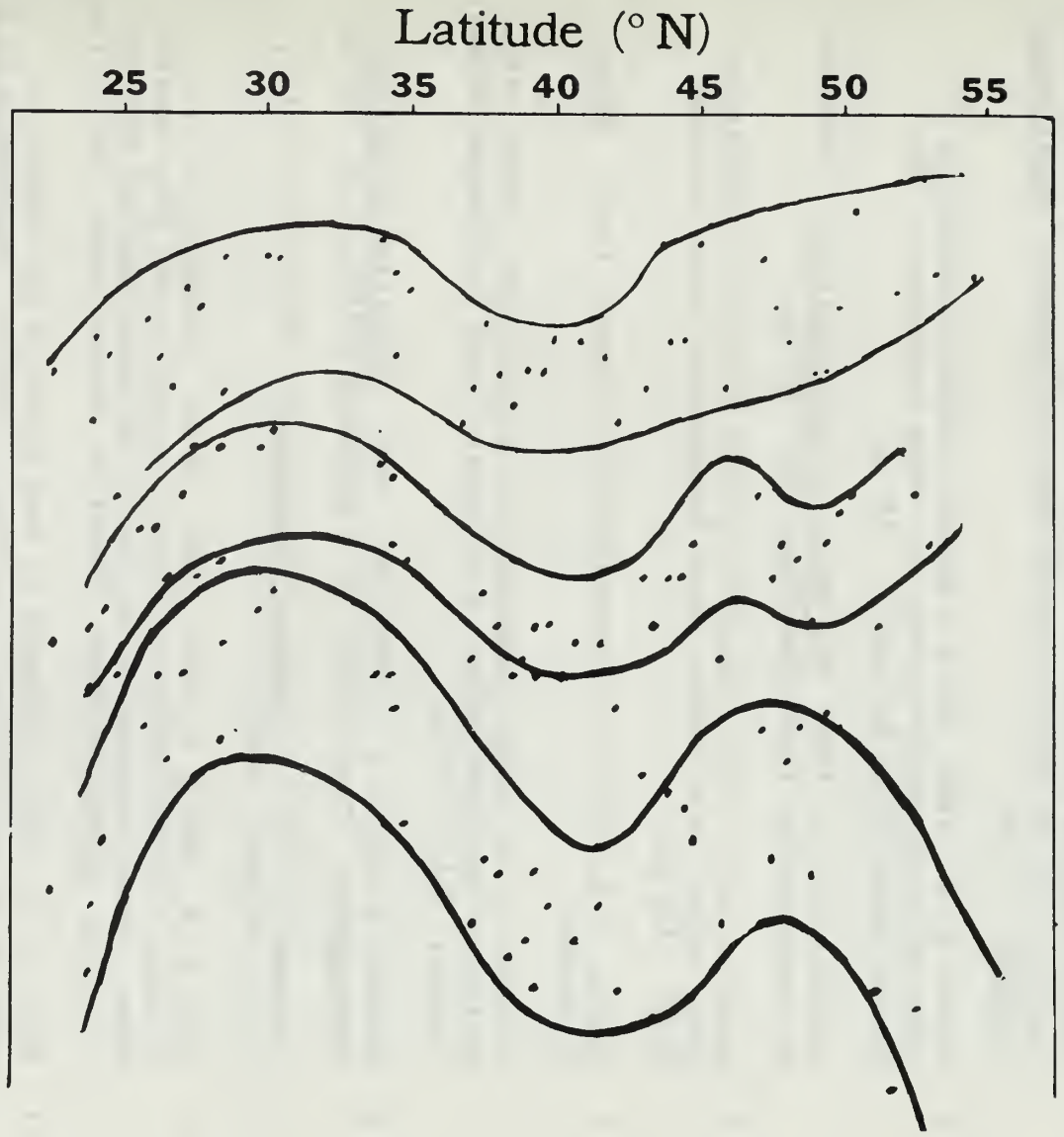

Figure 23. Thermocline Scatter Diagrams - 23 NOV 1968.

REFERENCES CITED

1. Boston, N.E.J. 1966. Objective definition of the thermocline. Ref. 66-19T, Department of Oceanography, Texas A&M Univ. 38 pp.

2. COMOPTEVFOR 1965. Operational evaluation of the AN/SSQ-36(XN-2) Bathythermograph Transmitter Set, the CV-801(XN-1)/ARR Signal Data Converter and the Anadex Converter-Rustrack Recorder. Final Report on O/V24. 37 pp.

3. Denner, W. W. 1969. The T-S gradient method, a new method of computing geostrophic currents over large ocean areas. Ph.D. Thesis, Oregon State University. 188 pp.

4. Greenspan, H. P. 1968. The Theory of Rotating Fluids. Cambridge at the University Press, Cambridge, Eng. 327 pp.

5. Grosfils, E. F. 1968. Objective digital analysis of bathythermograph traces. M.S. Thesis, Naval Postgraduate School, Monterey, Calif. 130 pp.

6. Knauss, J. A. 1957. An observation of an oceanic front. Tellus, 1, 94-101.

7. Moynihan, J. J. 1968. Investigation of geostrophic current calculations on the Grand Banks. M.S. Thesis, Naval Postgraduate School, Monterey, Calif. 62 pp.

8. Neumann, G. and W. J. Pierson, Jr. 1966. Principles of Physical Oceanography. Prentice-Hall Inc., Englewood Cliffs, N. J. 545 pp.

9. Proudman, J. 1953. Dynamical Oceanography. Methuen & Co. Ltd., London, England. 409 pp.

10. Reed, R. K., and N. P. Laird 1966. On the reliability of geostrophic flow determinations across a section of the North Pacific Ocean. Paper presented at the Pacific Northwest Regional Meeting of the Am. Geophysical Union, Corvallis, Oregon, August 1966. 11 pp.

11. Reid, R. O. 1959. Influence of some errors in the equation of state or in observations on geostrophic currents. Proceedings of a Conference of Physical and Chemical Properties of Sea Water. National Research Council, Washington, D. C., 10-29.

12. Snodgrass, J. M. 1966. Undersea Instrumentation Reliability: Where Away? IEEE Trans. Aerospace Electron. Syst. AES-2(6), 631-640.

13. Tabata, S. 1965. Variability of oceanographic conditions at ocean station "P" in the Northeast Pacific Ocean. Trans. Roy. Soc. of Canada, III(IV), 367-418.

14. Tully, J. P. 1964. Oceanographic regions and assessment of temperature structure in the seasonal zone of the North Pacific Ocean. J. Fish. Res. Bd. Canada, 21(5), 941-970.

15. Tully, J. P. and F. G. Barber 1960. An estuarine analogy in the Sub-arctic Pacific Ocean. J. Fish. Res. Bd. Canada, 17(1), 91-112.

16. Wyrtki, K. and V. Graefe 1967. Approach of tides to the Hawaiian Islands. J. Geophys. Res., 72(8), 2069-2071.

INITIAL DISTRIBUTION LIST

		No. Copies
1.	Defense Documentation Center Cameron Station Alexandria, Virginia 22314	20
2.	Library, Code 0212 Naval Postgraduate School Monterey, California 93940	2
3.	Oceanographer of the Navy The Madison Building 732 N. Washington Street Alexandria, Virginia 22314	1
4.	Naval Oceanographic Office Attn: Library Washington, D. C. 20390	1
5.	Assistant Professor N. E. J. Boston Code 58Bb Department of Oceanography Naval Postgraduate School Monterey, California 93940	2
6.	Assistant Professor W. W. Denner Code 58Dw Department of Oceanography Naval Postgraduate School Monterey, California 93940	1
7.	LCDR G. K. Gowans, USN Naval Oceanographic Office (Code 01812) Washington, D. C. 20390	1
8.	Department of Oceanography, Code 58 Naval Postgraduate School Monterey, California 93940	1
9.	Dr. B. P. Leonard, Jr. The Aerospace Corporation P. O. Box 950805 Los Angeles, California 90045	1

Security Classification

DOCUMENT CONTROL DATA - R & D

(Security classification of title, body of abstract and indexing annotation must be entered when the overall report is classified)

1. ORIGINATING ACTIVITY (Corporate author)	2a. REPORT SECURITY CLASSIFICATION
Naval Postgraduate School Monterey, California 93940	Unclassified
	2b. GROUP

3. REPORT TITLE

Variation in Thermal Structure and Geostrophic Current Between Alaska and Hawaii Determined from Synoptic Space Sections

4. DESCRIPTIVE NOTES (Type of report and inclusive dates)

Master's Thesis; October 1969

5. AUTHOR(S) (First name, middle initial, last name)

George Keith Gowans

6. REPORT DATE	7a. TOTAL NO. OF PAGES	7b. NO. OF REFS
October 1969	73	16

8a. CONTRACT OR GRANT NO.	9a. ORIGINATOR'S REPORT NUMBER(S)
b. PROJECT NO.	
c.	9b. OTHER REPORT NO(S) (Any other numbers that may be assigned this report)
d.	

10. DISTRIBUTION STATEMENT

This document has been approved for public release and sale; its distribution is unlimited.

11. SUPPLEMENTARY NOTES	12. SPONSORING MILITARY ACTIVITY
	Naval Postgraduate School Monterey, California 93940

13. ABSTRACT

Five synoptic space sections along 158°W longitude between Hawaii and the Aleutian Islands were developed from data collected by airborne expendable bathythermographs during experiment PARKA, a research project sponsored by the U. S. Navy in 1968. The sections are examined for spacial and temporal variation in thermal structure and geostrophic surface velocity.

Two recently developed analysis techniques are employed. Denner's T-S gradient method, wherein thermal and haline contributions to total geostrophic velocity are distinguishable, expedites calculations and results in velocity fields comparable to those developed by the dynamic method. Thermocline parameters are developed using Boston's objective definition of the thermocline, a statistical curve-fitting technique which develops the notion of a Gaussain thermocline.

Gross features of thermal structure remain fairly consistent during the heating season; however, thermal fronts are observed to vary in time and space. The distribution of isothermal lines with latitude suggests the possibility of a Taylor-column effect slightly north of Hawaii.

DD FORM 1 NOV 65 1473 (PAGE 1)

S/N 0101-807-6811

Security Classification

A-31408

14 KEY WORDS	LINK A		LINK B		LINK C	
	ROLE	WT	ROLE	WT	ROLE	WT
Synoptic sections						
158°W longitude						
AXBT						
Thermal structure						
Geostrophic surface velocity						
Gaussian thermocline						
T-S gradient method						
Taylor column						
PARKA						
Hawaii to Alaska						